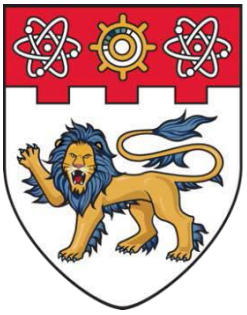

NANYANG TECHNOLOGICAL UNIVERSITY
SINGAPORE

IMPEDANCE SHAPING METHOD TO IMPROVE GRID CONNECTED INVERTER UNDER WEAK GRID CONDITION

ZHAO BOHUI

SCHOOL OF ELECTRICAL & ELECTRONIC ENGINEERING

2020

IMPEDANCE SHAPING METHOD TO IMPROVE GRID CONNECTED INVERTER UNDER WEAK GRID CONDITION

ZBH

2020

IMPEDANCE SHAPING METHOD TO IMPROVE GRID CONNECTED INVERTER UNDER WEAK GRID CONDITION

ZHAO BOHUI

School of Electrical & Electronic Engineering

A thesis submitted to the Nanyang Technological University

in partial fulfillment of the requirement for the degree of

Master of Engineering

2020

Statement of Originality

I hereby certify that the work embodied in this thesis is the result of original research, is free of plagiarized materials, and has not been submitted for a higher degree to any other University or Institution.

. . . . . .

21-MAR-2020

. . . . . .

ZHAO BOHUI

Supervisor Declaration Statement

I have reviewed the content and presentation style of this thesis and declare it is free of plagiarism and sufficient grammatical clarity to be examined. To the best of my knowledge, the research and writing are those of the candidate except as acknowledged in the Author Attribution Statement. I confirm that the investigations were conducted in accordance with the ethics policies and integrity standards of Nanyang Technological University and that the research data are presented honestly and without prejudice.

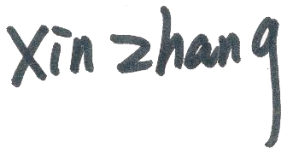

. . . . . .

29-MAR-2020

. . . . . .

ZHANG XIN

Authorship Attribution Statement

This thesis contains material from paper published in the following peer-reviewed journals where I was the first author.

Chapter 3 is published as **B. Zhao**, X. Zhang and L. Miao, "Adaptive Impedance Shaping Method for Improving LCL-type GCI under Weak Grid," 2019 IEEE 4th International Future Energy Electronics Conference (IFEEC), Singapore, Singapore, 2019, pp. 1-5.

The contributions of the co-authors are as follows:

The original idea was proposed by Prof. Zhang Xin and he also helped me revised the manuscript drafts. I finished the theoretical analysis and experimental verifications.

ZHAO BOHUI

. . . . . .

21-MAR-2020

. . . . . .

ZHAO BOHUI

Acknowledgements

Primarily, I would like to pay my authentic thankfulness to Prof. Zhang Xin who is the supervisor of my research during the long phase in writing this research report. To my best appreciate, I gratefulness him for the considerable patience in every scanning during this project and provided me effect persuasion towards entire research procedure. My professor always brings me generous assistance when many hint errors and tackles about the entire process. If there is no help from my supervisor, it was impossible for me to finish a report on an appropriate standard. Furthermore, his consideration for students, in reality, entitles him to be a totally good supervisor. The understandings for students and the spiritual encouragements are always available in support. It is my honor to have Prof. Zhang supervise me on my work. Thanks a billion.

Here I also want to thank those who have been encouraging me and supporting me all the time. Without their trust and help, I couldn’t have the strong motivation to urge me working hard on this dissertation. Thank you all.

Table of Contents

Abstract

Due to the popularity of renewable energy, e.g., wind power and solar energy, renewable energy generation systems(REGs) have been preferred as eco-friendly power generation systems. Distributed generation resources, including renewable energy sources, are essential for the distributed generation system. Grid-connected inverters(GCIs), as indispensable parts of the distributed generation system, are endangered by the non-ideal conditions. For instance, the harmonics, high impedance in weak grid condition, and instability issues caused by impedance mismatching.

In order to address the non-ideal conditions mentioned before, there are various improving technologies being modified to enhance the performance of grid-connected inverters. Generally, the LCL filters are applied between the inverter and the power grid to suppress the harmonics. However, the resonance circuit also leads to distortion and even instability issues. Therefore, the passive damping and active damping schemes are introduced in the topology of the inverter and control block. Besides, active power filters, unlike passive damping using passive damper, utilize active components to compensate for the harmonics and therefore eliminate the negative effect of harmonics. Nonetheless, the variable grid conditions and digital delay are still serious problems for the grid-connected inverter.

Firstly, unlike traditional active power filter, especially series active power filter, the adaptive controller for the APF model is required to improve the robustness in the variable grid conditions. According to model simplification, impedance-based stability criterion and bode plot analysis, it is indicated that the proposed control method certainly increases the phase margin and stabilizes the system in the ideal case. Eventually, the proposed series adaptive stabilizer is applied in the tested single-phase grid-connected inverter with a weak grid. Moreover, the experimental results are demonstrated, which prove the correctness of it.

Despite the active power filter, the active damping methods are widely applied in the inverter side to achieve the impedance shaping. Unlike the modified active power filter, the active damping method provides virtual impedance to shape the output impedance of inverter with no power loss. However, the negative effect of digital delay in the digital controller and the potential influence of weak grid condition are challenging the performance of control design. Therefore, the hybrid controller is applied and verified to be effective in eliminating the negative effect of digital delay and weak grid.

In this thesis, impedance shaping methods, including active damping and adaptive active power filter, are proposed and the performance of inverter will be improved.

As the limitation of single-phase inverter, the feasibility of the series adaptive active power filter should be investigated with new challenges. For future works, the application of series adaptive stabilizer will be discussed in three-phase inverter and parallel-inverter system, respectively.

List of Figures

List of Tables

List of Abbreviations

RES	Renewable Energy Sources
GCI	Grid Connected Inverter
PV	Photovoltaic
DG	Distributed generation
MCU	Microcontroller Unit
DSP	Digital Signal Processors
SPWM	Sinusoidal Pulse Width Modulation
FACTS	Flexible Alternating Current Transmission System
LFI	L-filter based Interleaved
GCFRS	Grid-Current-Feedback Resonance Suppression
CV	Capacitor Voltage
SMC	Sliding-Mode Control
APF	Active Power Filter
HAPF	Hybrid Active Power Filter
SVC	Static Var Compensator
UPS	Uninterrupted Power Supply
PLL	Phase-Locked Loop
PCC	Point of Common Coupling
SAS	Series-Connected Adaptive Stabilizer
SCR	Series-Connected Resistors
HIL	Hardware-In-the-Loop
ADNN	Adaptive Neural Network
PI	Proportional-Integral

Chapter 1 **Introduction**

This chapter begins with the introduction of the global renewable energy power system. With the rapid development of it, RESs gradually take the place of traditional power generation mode. Moreover, as an essential part of connecting RESs and power grid, grid-connected inverter is indispensable for distributed power generation systems.

However, the introduction of grid-connected inverter also causes harmonic and instability issues which are challenging for control design. Besides, the variable grid condition will deteriorate the case and lead to worse power quality. Although some control method is effective for improvement, most of the control method cannot handle variable grid condition, especially in weak grid condition.

Therefore, the thesis proposes two kinds of impedance shaping methods to attenuate harmonics, maintain stability and deal with variable grid conditions. The motivation of the research, the objectives, major contribution and organization of the thesis are presented as follows.

1.1 Motivation

Renewable technologies other than traditional biomass are often referred to as "modern renewable energy." Compared with traditional fossil fuel-based energy generation systems, RESs (renewable energy systems) are gradually preferred for the urge to build eco-friendly energy generation systems [1]. These include hydropower, the solar, wind, geothermal and modern biofuel production (including the conversion of modern forms of waste to biomass).

For instance, Fig.1-1 presents the changes and mix of modern renewable energy consumption, e.g., solar PV, wind power (as the main part of RESs) and other forms of RESs, over the past 50 years. 'Other renewables' refers to renewable sources including

geothermal, biomass, waste, wave and tidal. Traditional biomass is not included. The unit in the chart is terawatt-hours (Wh) per year (TWh/y). Moreover, it can be viewed in most of the countries and different regions. Fig. 1-1 is an overview of it and integrates all the data.

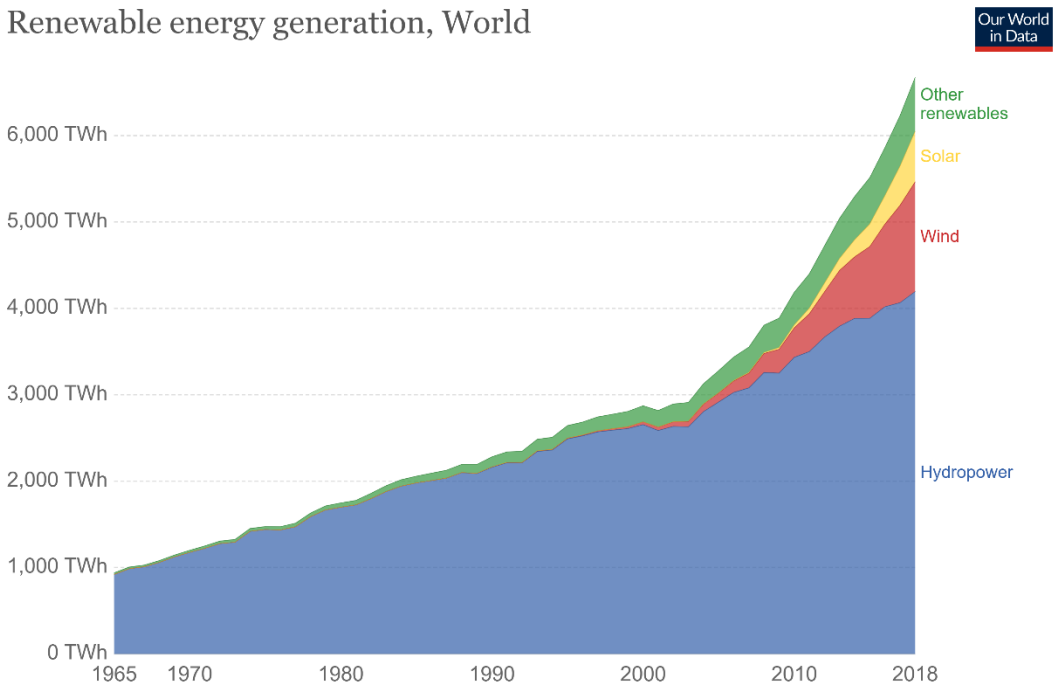

Fig. 1-1. The change & mix of modern renewable generation, 1965-2018(Statistic Review of Global Energy [Online]. Available: ourworldindata.org).

Globally, approximately 5900TWh of modern renewable energy was produced worldwide in 2016. This is a five- to six-fold rapid increase since the 1960s. Fig. 1-2 presents the share of each kind of modern renewable energy generation. As shown in Fig. 1-2, we can see that hydropower is still the leading form of modern renewable energy consumption, accounting for nearly 70%.

Even though the absolute increase in production, the share of hydropower is declining with the development of other renewable energy technologies. From the chart, it is suggested that modern renewable energy, especially solar PV and wind power, has increased rapidly. For solar PV, the share of it in global renewable energy consumption

grew to nearly 9% in 2018. Similarly, the share of wind energy in global renewable energy consumption grew to 19%. However, the share of hydropower has decreased from 80% in 2011 to 63% in 2018. These data derived from the chart indicates the growing importance of RESs.

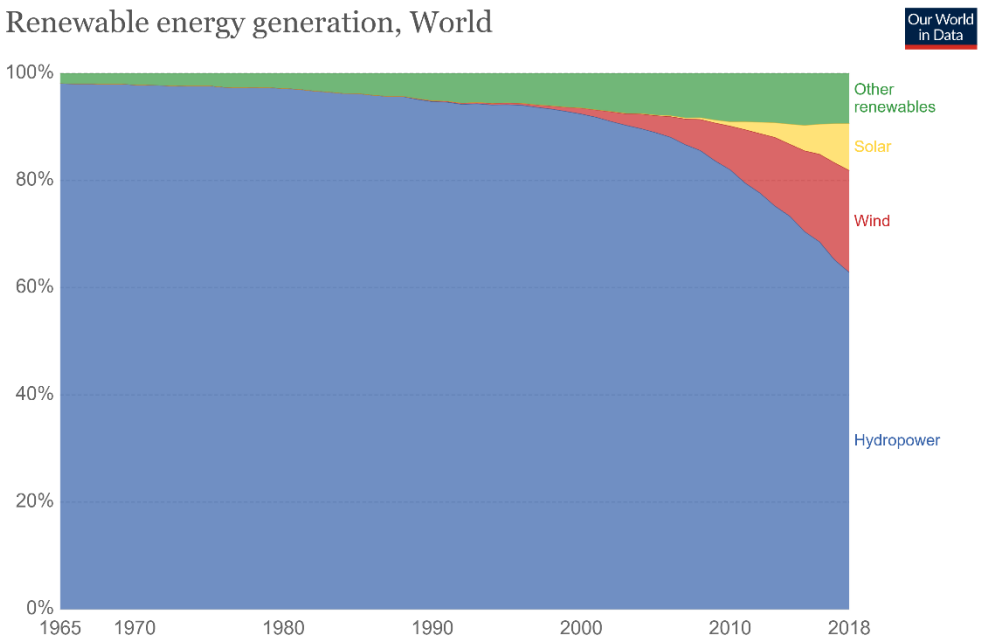

Fig. 1-2. The share of each kind of modern renewable energy generation, 1965-2018(Statistic Review of Global Energy [Online]. Available: ourworldindata.org).

In order to achieve power transformation between RESs and utility grid, grid-connected inverter can be applied to converts DC power into AC power in a suitable way for injecting into the power grid. Generally, as the interfaces between local electrical power generators, e.g., solar panel, wind turbine, hydro-electric and the utility grid, GCIs(grid-connected inverters) plays an indispensable and leading role in injecting high-quality power, ensuring power security, safe operation and also providing support to the grid side[4].

For instance, Fig.1-3 presents the schematic diagram of a basic PV generation system. The basic system, which including PV panels, a grid-connected inverter and the power grid, converts the DC power in solar PV generation system into AC power and injects

the AC power into the grid[6].

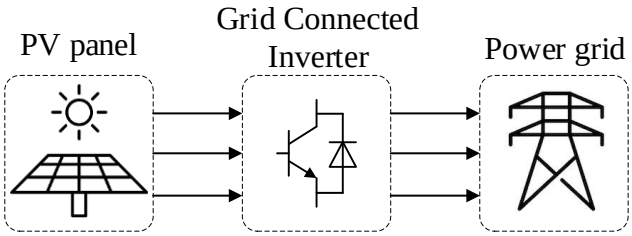

Fig. 1-3. Schematic diagram of a basic PV generation system

The schematic diagram of a basic wind power generation system is depicted in Fig.1-4. As shown in the figure, the wind power firstly needs to be transformed into DC power. The wind turbine may have the output of a small wind turbine with an AC voltage that changes the value of frequency and voltage depending on the speed of the wind. In this case, an AC/DC converter is needed. Once the AC/DC stage is included, the grid-connected inverter will connect the output of the converter and the power grid.

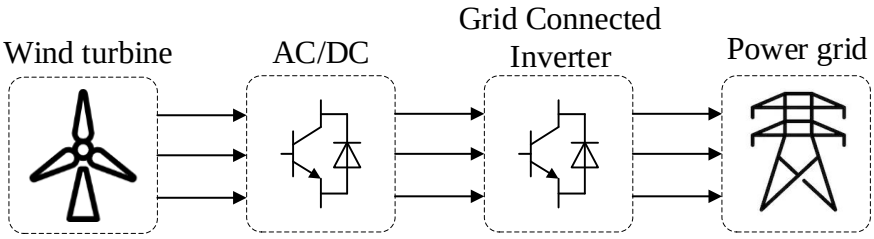

Fig. 1-4. Schematic diagram of a basic wind power generation system

According to the discussion above, GCI indeed plays a dominant role in the distributed power generation systems(DGs). However, there are lots of problems to be solved when applying GCI. One of the issues is the harmonics. The output current of the grid-connected inverter always contains different orders of harmonics which will significantly deteriorate the power quality[5]. Thus, to achieve the reduction of current harmonics and improve power quality, various kinds of filters are applied in the topology of the GCIs. For example, L filter, LC filter, LCL filter and LLCL filter are typically employed in grid-connected power conversion system[14]. Besides, to realize the superior effect of

mitigating harmonic components, we usually adopt high-order passive filters including LCL filters and LLCL filters. However, companying with high-order passive filter, the introduction of them will trigger resonance because of the interaction with grid components. In this case, more harmonics at the resonant frequency will be magnified and then aggravate the power quality and even affect the stability of the inverter since the existence of resonance circuits.

Weak grid condition causes another issue. In the process of power transmission, the DGs may be remote from the load side (utility grid). Therefore, long transmission lines will introduce an equivalent variable impedance to the power grid[4]. Under the weak grid condition, the power quality and even the stability of the grid-connected inverter will be influenced[7]. Therefore, optimizing the control method to fit variable grid conditions is gradually on the rise.

1.2 Objectives

In order to address the harmonics issue in the design of grid-connected inverter as well as the instability issue caused by weak grid condition, various optimizing approaches are proposed to achieve the improvement which will be reviewed in detail in the next chapter.

Generally, there are mainly two kinds of control methods to realize the goal. One is the passive damping method, the other is the active damping method[9]. For the passive damping method, it is widely applied in the topology of the passive filter. As a reasonable improvement to attenuate harmonics, it has a practical effect. However, the shortcoming of power loss is also regarded as a limitation. For active damping methods, since they do not consume power, most of the control loop contains the active damping method rather than the passive one[10].

Although being widely used for harmonics reduction, the grid-connected inverter is still facing instability issues under weak grid conditions. Because the fast implementation of

various digital signal processing algorithms are more effective in establishing a control model than analog control, more digital controllers are applied in the control of inverter. For example, lots of researches used microcontrollers(MCU) and DSP to control inverter based on SPWM (sinusoidal pulse width modulation) technology[18]. In this case, digital delay, which is a normally ignored factor, needs to be considered in the control design[11]. Specifically, digital delay shows even more severe side effects in weak grid condition which will lead to instability issues.

Power electronic converters are the sources of harmonic generation in RESs generation. However, the same can be used to mitigate the harmonics in the system, such as FACTS Devices, active filters, etc.[15]. No matter applying an active damping method or passive filter, the control method can only be used in a certain grid condition. Thus, the design of the control loop requires more parameters, such as parameters of the inverter. This will be difficult to design and apply. In addition, the control loop must be designed based on the changes in GCI.

For the active power filter, it has superior suppression on harmonic components when the system stability is promised. However, in weak grid condition, the performance of the active power filter will be influenced and cause instability issues.

In summary, in order to fill the research gaps as mentioned earlier, the thesis aims at optimizing the control method which is relative to impedance shaping methods.

1.3 Major Contribution of the Thesis

This thesis proposes the impedance shaping methods to address both the harmonics and instability issues. The major contributions can be summarized as follows:

(1) Due to variable grid conditions, the robustness of the control model is essential in the design procedure of inverters. According to the impedance-based stability

criterion, the impedance shaping method can be applied to the grid side. The series-connected adaptive stabilizer, which is similar to active power filter, can attenuate harmonics and improve the stability successfully.

(2) The impact of the weak grid and digital delay on the grid-connected inverter has been discussed at the beginning. Moreover, a hybrid control method, including digital controlled feedback and analog controlled feedforward, has been proposed to address both the harmonic and instability issues caused by digital delay and weak grid condition.

1.4 Organization of the Thesis

The following of the thesis is organized as follows:

Chapter 2 introduces different kinds of grid-connected inverter, such as L type, LC type and LCL type. Moreover, it reviews the existing improving optimization methods including passive damping method, active damping method and active power filter.

Chapter 3 discusses the basic modeling simplification of a certain kind of GCI topology(LCL type GCI) and its stability under weak grid condition at the beginning. The small-signal model of the inverter with the weak grid is derived from the theoretical discussion. Then, the impedance-based stability criterion is introduced and applied to analyze the stability of the GCI with a weak grid. Moreover, this chapter investigates the impedance shaping method for the grid side impedance. This chapter studies an adaptive impedance shaping method called series-connected adaptive stabilizer(SAS) to improve the stability of the system. The proposed control model can fit into various grid conditions. At last, experimental verifications are provided, which are consistent with the theoretical analysis.

Chapter 4 investigates the impedance shaping method for the inverter side. Instead of shaping the grid side impedance, this chapter discusses the output impedance of inverter

to suppress the harmonics as well as improve the stability of the system. The impacts of digital delay effects are discussed and analyzed in the design of the control loop. Subsequently, an improving hybrid control method is proposed to enhance the stability of GCI with a weak grid. Finally, experimental verifications are presented, which are consistent with the theoretical analysis.

Chapter 5 concludes the thesis and suggests some possible future research works.

Chapter 2 **Literature Review**

As discussed in the introduction chapter, the goal of suppressing the harmonics as well as maintaining system stability is urgent for inverter optimization. Therefore, in order to deal with the harmonic issue and instability issue, various improving approaches have been presented. In this chapter, the control methods of grid-connected inverter will be briefly reviewed and discussed.

2.1 Grid-Connected Inverter

To begin with, the grid-connected inverter needs to be introduced. Firstly, inverters are used for energy conversion from DC source to AC output, both in a standalone mode or when connected to the utility grid. As for grid-connected inverters, similarly, they are interfaces to connect renewable energy sources to the power grid[12].

However, there are two kinds of harmonic issues when the inverter is connected to the power grid. Firstly, as intermittency of renewable energy sources, especially for solar PV system and wind farm, the output of RESs are significantly subject to solar irradiances and wind speeds, respectively[12]. Therefore, when connected to the power grid through GCI, the intermittency of the renewable energy sources may lead to high-frequency switching of power electronic devices in the inverter. In this case, the output current injected into the power grid will be distorted because of the generation of high-frequency harmonics. Furthermore, the power quality will be deteriorated as well. Besides, the nonlinear load at the grid side will also cause harmonic issues[15].

As previously discussion of harmonic issues, a variety of improving methods to mitigate harmonics. Due to the characteristics of output components, different passive filters are widely used at the output port of the inverter. Nonlinear devices can effectively suppress high-frequency components and therefore applied in the design of passive filters. Fig.2-1 presents the four main types of passive filters.

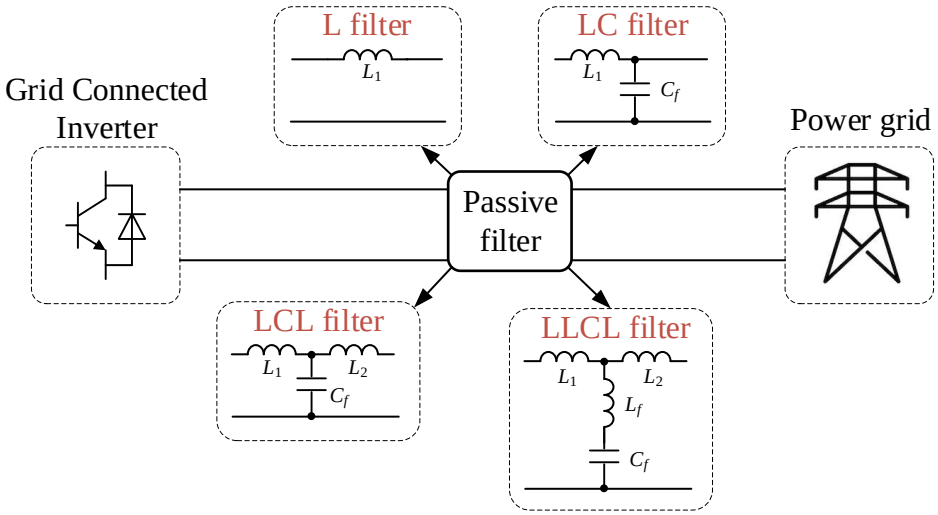

Fig. 2-1. Passive filter

Generally, there are three basic kinds of passive filters. As shown in Fig. 2-1, L filter is the most simple filter since its topology only contains a filter. Usually, in the output of the inverter, LCL filters are widely used as passive filter topology because of superior suppression on harmonics[14].

Firstly, the most simple filter is the L-type filter. As known, the output of the inverter contains the DC component and AC component. For DC input, inductor acts as short-circuit hence DC components that are coming out of the inverter would get dropped directly across the load side and no voltage drop of any sort across the inductor. The L filter is to limit the circulating current (which will appear as current harmonics) that would arise due to the instantaneous difference in waveform between the sinusoidal grid voltage and the PWM inverter voltage. [18] utilizes an L filter at the output of the inverter. Besides, the control loop of the inverter is achieved in the DSP through a novel predictive current control. However, the L-filter cannot handle variable conditions because filter inductance mismatch leads to distortion or even more severe issues. In [19], the mathematical model of an L filtered VSC(voltage source converter) is derived from achieving the linearization of both the inverter and feedback control. [20] compares the conventional LCL filter and L filter. From the practical function, L filters have the advantage of low cost. Therefore, the author proposes a new multi-interleaved technique

with the application of L filter called L-filter based interleaved (LFI). In [21], the author discusses the dynamic effects of the inverter with L filter which reveals the limitations of L filter. Based on the analysis of harmonics, inductor saturation and even dead-time nonlinearity, the paper summarize the factor that would lead to severe instability issues. [22] presents the need to improve stable margin and power quality of the L type grid-connected inverter. Moreover, this paper proposes a virtual high-frequency damping method as an active damping method, which will be discussed later.

LC filter includes an inductor at the inverter side and a parallel-connected capacitor. Therefore, the LC filter is regarded as a second-order output filter. When designing the parameters of the LC filter, the most important one is the cut-off frequency which is relative to the existence of the resonance circuit. Besides, the quality factor of the LC filter, which will affect the frequency response of the filter, is always selected for critically damped in order to obtain flat passband and phase response.

In [23], the transient characteristics of the LC filter in a discrete state is taken into consideration. Through improving the modeling of three-phase LC type inverter, the deadbeat controller improves the power quality and stabilize the system. In [24], the author summarizes the advantages and shortcomings of LC filter. As the most cost-effective passive filter, it has a superior ability to eliminate harmonics than L filter. However, the resonance of filter may lead to over-voltage. This paper proposes a detailed filter design dealing with suppression of dv/dt. [24] investigates the design procedure of the LC filter in both off-grid and on-grid conditions. Moreover, the author introduces a passive damping method to ameliorate the performance of LC filter. In [26], the performance of LC filter is analyzed in the solar PV system. Similarly, it presents the analysis of LC filter under the transient case. To overcome the issues, the author utilizes series-connected RL choke to eliminate the side effects.

Compared with a first-order L filter and second-order LC filter, an LCL filter can better

decouple between inverter and power grid. Since it is a third-order filter, the attenuation of the LCL-filter is 60 dB/decade for frequencies above the resonant frequency. Therefore, lower switching frequency for the inverter can be used. It also provides better decoupling between the filter and the grid impedance and reduces the current ripple on the grid inductance. Even with a small inductance value, the LCL filter has good current ripple attenuation. Therefore, the LCL filter is suitable for most applications.

However, the topology of the LCL filter indeed introduces the resonant issues which would make the entire system vulnerable. This resonance effect can cause instability voltage or current around the resonant frequency. It will also bring resonances and unstable issues in the system. Hence, the filter needs to be designed precisely according to the parameters of the specific converter. In specialized writing, we can discover numerous articles on the structure of the LCL filters. A significant parameter of the LCL filter is its cut-off frequency. The cut-off frequency of the filter must be minimally one half of the switching frequency of the converter because the filter must have enough attenuation in the range of the converter's switching frequency.

In [27], the limitations of the LCL filter are reviewed. Besides, the author optimizes the design procedure of the LCL filter in order to minimize the value of the inductor and capacitor. [28] details the optimal design of the LCL filter. Compared with traditional try and error, the proposed optimal is designed to meet the certain grid regulations and reduce the total filter inductance in the meanwhile. [29] also presents a detailed design procedure of inverter-side inductor, capacitor and grid-side inductor, respectively. Inverter-side inductor L_1 is designed according to power loss and size tradeoff. The rest of the filter components are designed according to the attenuation requirements.

In [30], the parameter design of the LCL filter and requirements is discussed in grid-connected condition. Most importantly, the selection of ratio between the grid-side inductor and inverter-side one is detailed in the paper. In [17], the passive filters including

LCL filter are reviewed. The author proposes the passive damping method, which will be discussed later, to improve the performance of passive filters. [31] presents the approach of designing inverter and output filter with consideration of stability and system robustness requirements. In [32], a novel deadbeat control method is introduced in the LCL type GCI. The improving method is derived from the z-domain instead of the s-domain in the GCI. Based on the above introduction, it is proved that the design of the LCL filter contains lots of limitations which are complicated. Even though the LCL shows superior ability to attenuate the harmonics, most of the case studies adopt other kinds of improving methods to achieve the desired attenuation as well as stability. [10] also illuminate the effect of power loss in the process of design.

2.2 Damping Methods

2.2.1 Passive Damping Method

Generally, the passive damping method has the following methods: damping resistor in series with the filter capacitor, additional parallel R_dC_d damper, LCL with trap and series damping resistor [25]. The common passive dampers are illustrated in Fig.2-2. However, the resistor value has impacts on the filter response, voltage and current harmonic distortion and system power loss. Therefore, it will affect the efficiency of the GCI.

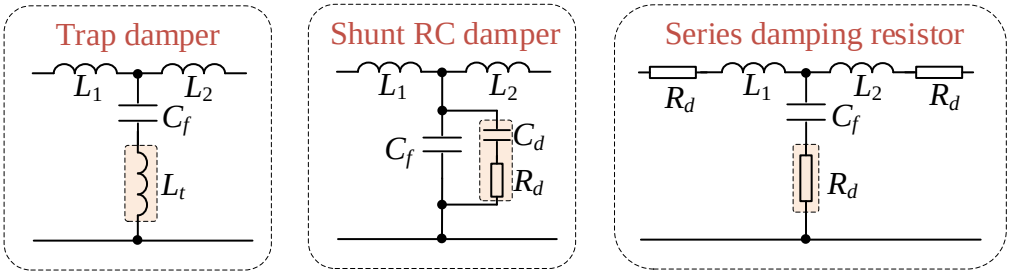

Fig. 2-2. Passive damping methods

In [33], the advantages and shortcomings of passive damping are reviewed. The author proposes an optimal design method to minimize the filter resonance as well as passive

damping value. The paper utilizes the LCL filter with LC traps. [34] presents and compares two widely used passive damping methods, series R damped and shunt RC damped. The analysis concentrates on the following aspects: resonance damping, current harmonics attenuation and power loss of damping. Most importantly, the power loss of passive damping is a critical challenge which is also proposed in [10].

In [35], the LLCL type grid-connected inverter with a passive damping method is proposed in a stiff grid condition. It also indicates the advantage that the passive damping method is preferred for simple design and low cost in stiff grid condition. [36] presents a split-capacitor resistive-inductor(SC-RL) passive damping method. Based on conventional RL damper, the proposed method significantly reduces power loss and make it suitable for high power application.

In [37], several kinds of passive damping methods are reviewed. For instance, series RL damper, shunt RC damper and series damper Moreover, the hybrid damping method is also discussed. [38] utilizes a certain passive damping circuit and combines it with the topology of the LCL filter. However, the complexity of the designed passive damping circuit is the limitation in the process of application.

2.2.2 Active Damping Method

The active damping method suppresses the resonance by increasing the damping coefficient of the filter by adding feedback signal to the control section.

Generally, the additional control loop is introduced by adding one of the state variables in the control method, such as the capacitor current, in order to develop a virtual resistor. Since there is no actual resistance element, the filter does not generate additional losses in electrical energy. It not only optimizes the power quality, but improves the efficiency of the inverter as well.

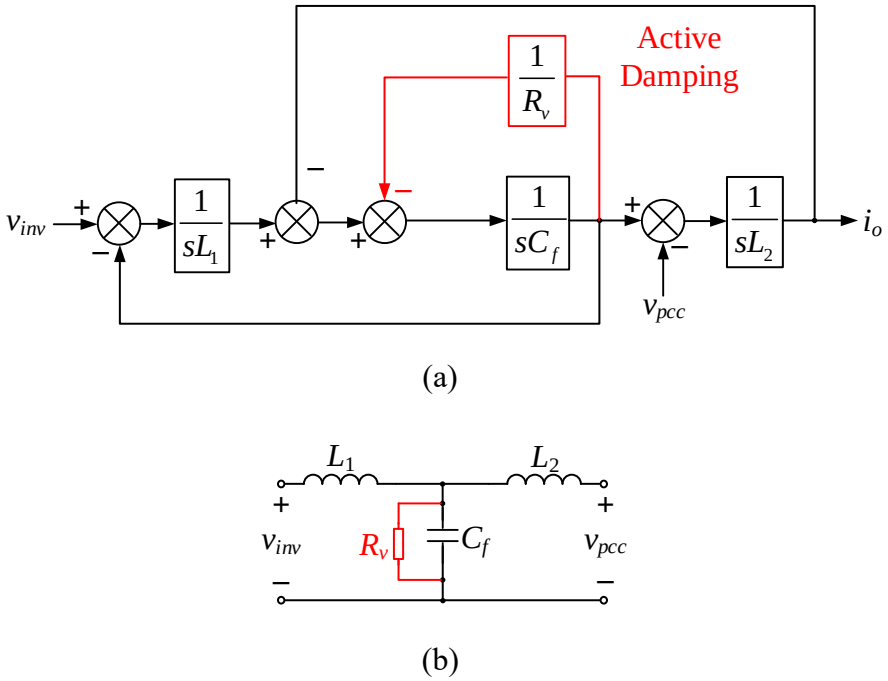

Fig. 2-3. (a)Active damping in the block diagram of LCL filter (b) Equivalent circuit of active damping

As shown in Fig.2-3(a), the function of the active damping method is equivalent to the passive damping method while it causes no power loss. For instance, the active damper is designed to be a resistor parallel-connected with the capacitor. The equivalent circuit is shown as Fig.2-3(b).

The most simple active damping method only contains a single loop. In [39], a filter-based active damping method is proposed to attenuate the harmonic components. The filter-based active damping method is achieved by the current control loop. [40] presents a novel active damping method without any redundant current sensors. The proposed control loop does not need to use the sensor to sense the capacitor current.

In [41], a novel notch filter-based active damping method is proposed. Most importantly, the proposed method achieves robust active damping and obtain superior ability to attenuate harmonics and maintain stability. In [42], a robust grid-current-feedback resonance suppression(GCFRS) method is proposed in the variable grid condition, especially in the weak grid.

Another type of active damping method includes multiple loops. [43] introduces specific guidelines to design the parameters in the control loop of the capacitor-current-feedback active damping method. In [44], based on the limitation of the capacitor voltage(CV) damping method, an additional feedforward compensator is introduced in the control loop. In [45], LCL filter resonance is divided into three specific regions. It is indicated that the active damping method is not required in the high-frequency region while it is indispensable in the low-frequency region.

Moreover, some active damping method contains a complex and distinct structure. [46] presents a multi-resonant state-space controller to realize the desired capability of attenuating harmonics and robustness. [47] introduces a predictive control method to achieve a fast response. Besides, the proposed method use grid voltage estimator and state observer to eliminate noise caused by sensors. In [48], a sliding-mode control(SMC) method is improved by introducing multiple resonant terms of grid current error into sliding function. The proposed scheme can suppress the current harmonics and fit the changing parameters.

2.3 Active Power Filter

Active power filters(APF) are power electronic devices dedicated to improving power quality and efficiency[15]. There are three types of active filters: shunt APF, series APF, and hybrid APF[49].

The topologies of these three kinds of active power filters are presented in Fig. 2-4. In Fig.2-4(a), series APF is series connected with the GCI and power grid while the shunt APF is parallel connected with the GCI and power grid. As for hybrid APF, it combines active power filter and passive filter at the same time. The simple topology of it can be depicted as Fig. 2-4(c).

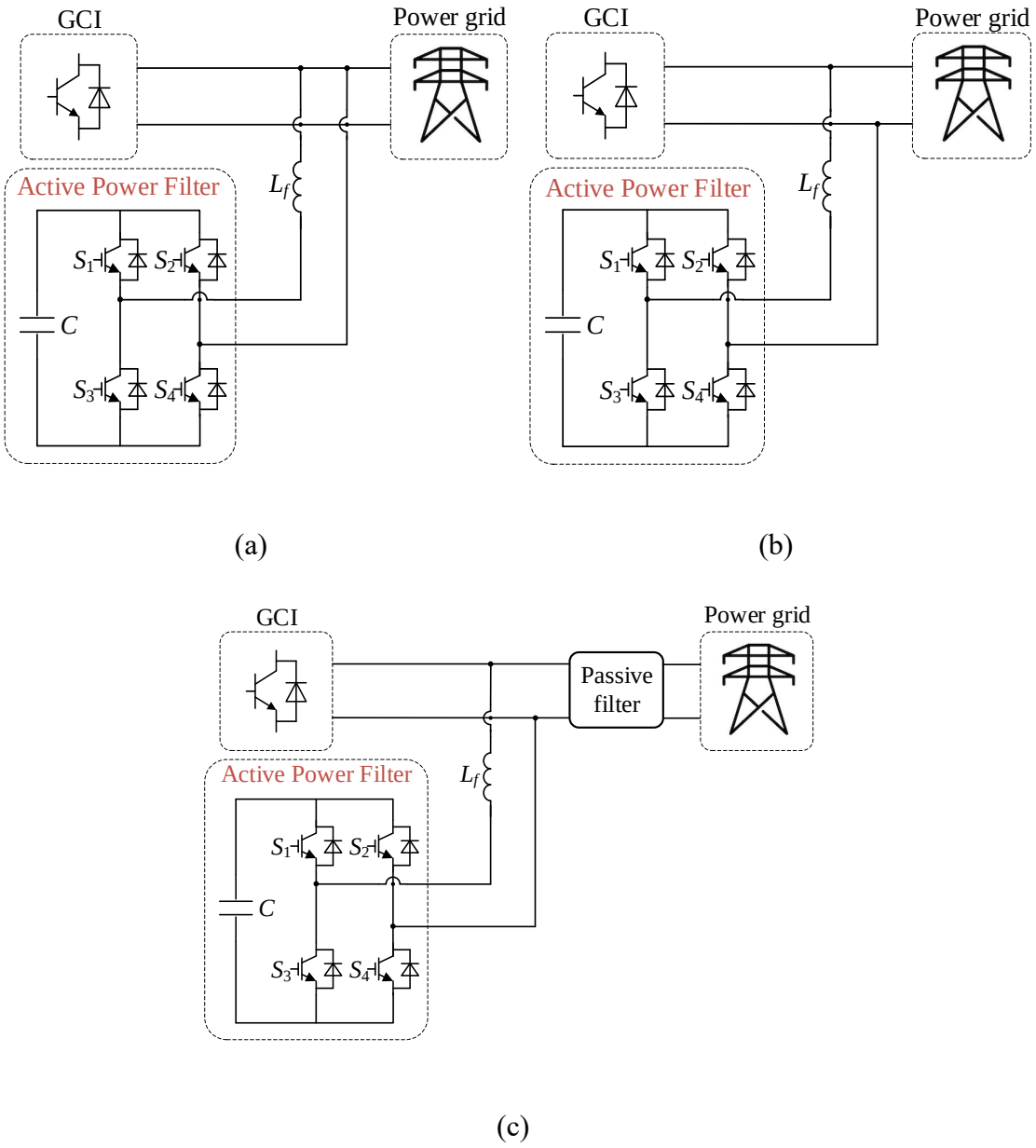

Fig. 2-4. Active Power Filter types: (a)Series active power filter; (b) Shunt active power filter; (c)Hybrid active power filter(Shunt APF+Passive filter).

The series APF apply a high impedance current path to the current harmonics in order to compensate for the current distortion caused by the nonlinear load. It will force high-frequency components to flow through the LC passive filter, which is in parallel with the load. In [50], a hybrid control method is introduced in series APF. The author combines two different control methods, including detecting source current in the closed-loop system and detecting load voltage in the open-loop system. In [51], the control scheme and operating principle are presented. Moreover, the proposed control method is proved

to be effective and robust in different load conditions.

The shunt APF injects equal but opposite harmonic current to compensate current harmonics. In this case, the shunt active power filter is regarded as a current source. The harmonic current generated by shunt APF will cancel the effect of current harmonics of the load side. In [52], a Kalman filter-based adaptive method is proposed to obtain the reference value of compensating current. The proposed control scheme significantly improves the dynamic performance of shunt APF. [53] proposes neural filtering-based shunt APF for compensating current harmonics. The current reference value is obtained from a notch filter based on the linear adaptive neuron.

The hybrid APF combines the advantages of the above kinds of active power filter[54]. It includes active and passive filters with series and parallel topologies, for instance, an active power filter in series with a passive shunt filter. Comparing with previous kinds of APF, hybrid active power filter(HAPF) is widely applied in the topology of GCI. In [54], a shunt APF combining with a passive LC filter is proposed to improve the capability of compensation and suppression on parallel resonance. [55] proposes a hybrid series passive LC filter with a shunt APF system which can be applied in high power condition.

However, it is indicated that the high-frequency switching requires a high-speed embedded controller. [56] proposes a novel model of static var compensator(SVC) in parallel with a HAPF. The introduction of SVC can compensate for the shortcoming of passive LC filter and attenuate the active inverter current. In [57], the control method in HAPF is improving as three-phase three-wire thyristor-controlled LC coupling. The proposed TCLC control provides different firing angles for each phase of the coupling part under unbalanced loading.

2.4 Digital Delay

In [59], the effect of digital delay on the performance of the inverter is reviewed in detail. As for the application of the digital controller in an uninterruptible power supply(UPS) based inverter, the author modifies the traditional PWM technology to fit the computation delay and sampling delay. The proposed PWM technology with two polarities(active-low and active-high) and realized it with the asymmetric scheme. [60] presents two current control loop(inverter current and grid current) in order to achieve the better capability of suppressing harmonics and considers the time delay using Taylor expansion. Similarly, the model of time delay can be linearized as one and a half sampling time step. In [61], the effect of transport delays is discussed. Moreover, a modified digital controlled current controller is proposed to improve the performance of the derivative part. Therefore, the negative influence of transport delay is attenuated.

In [62], the effects of digital delay are comprehensively investigated for a single control loop in two conditions. On the one hand, the existence of time delay will lead to instability problems in the inverter current-controlled feedback loop. One the other hand, with regard to the grid current controlled feedback loop, the time delay will improve the control loop in some extents.

[63] demonstrates the control design in the discrete time domain including the discretized model of time delay. Besides, the control frequency is investigated combining with topology and parameters of LCL filter in order to obtain better stability margin, wider system bandwidth, and excellent dynamic performance. In [64], the digital differentiator is realized in a discrete time domain with both first-order and second-order. In [65], the computation delay, PWM control delay and effect of PLL are considered in the design of a novel impedance phase compensator to shape the output impedance of the inverter side.

In [66], the effect of delay is discussed in the application active damping method. A novel impedance cancelation is proposed to eliminate the negative effect of variable grid impedance. It is indicated that digital delay can be significantly attenuated in the impedance cancelation.

As the discussion above, if the digital delay needs to be considered when the digital controllers are applied in the control system. On the one hand, since the digital controller is much more prominent, the fast speed to process data has been preferred to achieve the better performance of the controller. On the other hand, the introduction of a digital controller probably leads to instability issues caused by digital delay.

2.5 Weak Grid Effect

The weak grid means that the voltage at the connecting point will be very sensitive to any variation of the load[8]. For example, a microgrid can be regarded as weak grid condition[69]. The voltage of PCC usually contains a variety of different voltages of background harmonics, caused by nonlinear electronic components[33]. The load current flows through the grid impedance(nonlinear). Therefore, the harmonic level in weak grid conditions is usually much higher than that in a stiff grid.

It has been pointed out that even small levels of grid voltage harmonics can significantly distort the injected grid current and deteriorates power quality [67]. Moreover, the dynamic performance of the inverter may be effected. Besides, the injected harmonics, the oscillation of current and voltage waveforms, and the stability of the system may become severe issues because of a series of DER units. Thus, the grid-connected inverter should also be designed with high harmonic- rejection-ability, so as to meet stringent limitations on the harmonics of injected grid current.

Generally, a large and stiff power grid can be regarded as an ideal voltage source, the output impedance can be regarded as zero. However, a weak grid is not and the grid

impedance cannot be ignored. According to (5), the existence of Z_{oC} affects output current because the current is relative to the voltage harmonics.

Chapter 3 Series-connected Adaptive Stabilizer

This chapter focuses on the adaptive impedance shaping method which shapes the grid equivalent impedance. In the beginning, the modeling of the LCL-type grid-connected inverter with a weak grid simplifies the implementation of the control method. Then, in order to analyze the stability of GCI with a weak grid, the impedance-based stability criterion is introduced for stability analysis.

To address the instability issue which cannot be solved by the series active power filter, the proposed impedance shaping method is discussed in the ideal case to reveal the ideal function of it. Through the Bode plot in the ideal case combining with the original system, the proposed method can fix the instability issues caused by a weak grid if designed well.

Therefore, the Series-connected Adaptive Stabilizer (SAS) is introduced as a novel impedance shaping method. The basic topology, which is similar to series active power filter(APF), is discussed and then the schematic of GCI with a weak grid after introducing it is specified. Through the Bode plot in the real tested system, it is verified that the proposed SAS model indeed improves the stability of the inverter with a weak grid. Finally, experimental verifications are presented, which are consistent with the theoretical analysis.

3.1 Model simplification

3.1.1 Simplification Process

In the process of improving the performance of inverter, simplification is needed to be specified in the following reviews at the beginning. Firstly, the LCL filter and inverter model is reviewed. The basic topology of a single-phase LCL-type grid-connected inverter is shown in Fig.3-1.

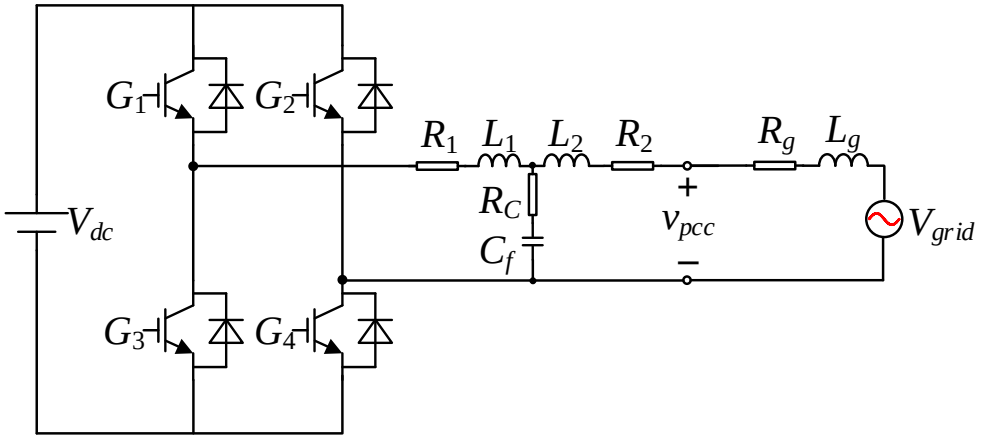

Fig. 3-1. LCL-type GCI with weak grid

As seen in Fig.3-1, the LCL -type inverter is series connected with the grid. V_{dc} denotes the DC voltage source. Four gate signals (G_1-G_4) to control the switching of IGBT are generated by the PWM generating circuit. The LCL-type filter consist of two inductors and a capacitor which refers to L_1, L_2 and C_f. The series-connected resistors(SCR) refer to R_1, R_2 and R_f, which are series-connected with these non-linear devices. L_g and R_g represent the impedance on the grid side. V_{grid} denotes the grid voltage source.

In order to simplify the whole model, the topology circuit of the LCL type filter is proposed in Fig.3-2 as a two-port network. Therefore, the filter can be treated as a black box.

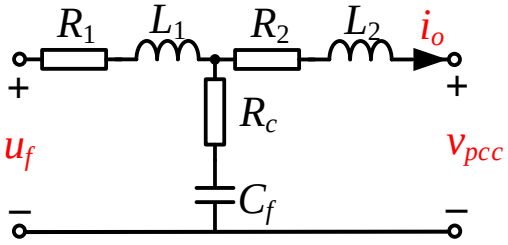

Fig. 3-2. Topology of LCL filter

u_f refers to the input voltage of the LCL filter, which is equal to the output voltage the inverter, and v_{pcc} refers to the voltage of point of common coupling(PCC), which represents inverter output voltage and output voltage of the LCL filter respectively.

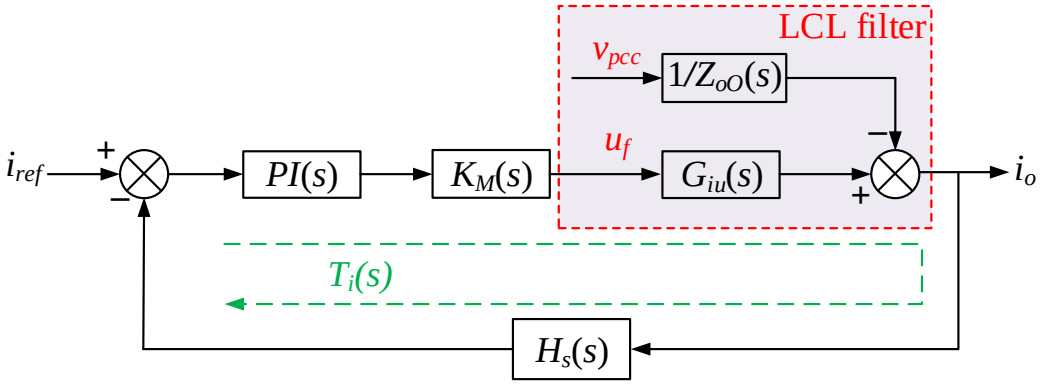

Fig. 3-3. Block diagram of LCL type GCI

Moreover, the block diagram is depicted to generalize the whole system in Fig.3-2, which is shown as Fig.3-3. The system will be introduced with a simple current-controlled feedback loop as a controller block. K_M(s) denotes the index of modulation and T_i(s) refers to the loop gain of the closed loop. PI(s) denotes the transfer function of the PI controller.

$$K_M = \frac{V_{dc}}{V_{tri}} \tag{3-1}$$

$$\begin{aligned} T_i(s) &= PI(s) \cdot K_M(s) \cdot G_{iu}(s) \cdot H_s(s) \\ &= \left(K_p + \frac{K_i}{s} \right) \cdot K_M(s) \cdot G_{iu}(s) \cdot H_s(s) \end{aligned} \tag{3-2}$$

$H_s(s)$ refers to current coefficient of feedback loop.

As seen in the Fig.3-3, LCL filter can be simplified as two different transfer functions G_{iu}(s) and Z_{oO}(s) which represent the filter output current to input voltage transfer function and open-loop output impedance. These two transfer functions can be derived by changing control variables. The specific procedures are shown as Fig.3-4 and Fig.3-5:

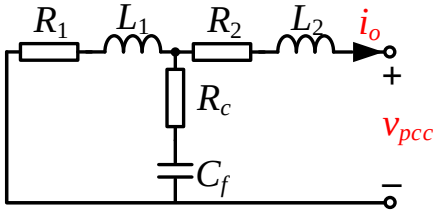

Fig. 3-4. Equivalent circuit of Z_o

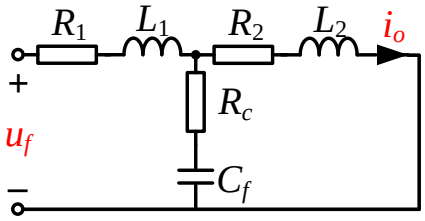

Fig. 3-5. Equivalent circuit of G_{iu}

According to the above figures, when u_f and v_{pcc} are controlled to be zero(short circuit), respectively, the two transfer functions can be easily derived from the topology. G_{iu}(s) can be expressed as (3-3) by setting v_{pcc} to zero. Z_{oO}(s) can be expressed as (3-4) by setting u_f to zero:

$$G_{iu}(s)=\left.\frac{\hat{i}_o}{\hat{u}_f}\right|_{\hat{v}_{pcc}=0} =\frac{1/sC_f+R_c}{(sL_1+R_1)\cdot(1/sC_f+R_c)+(sL_1+R_1)\cdot(sL_2+R_2)+(1/sC_f+R_c)\cdot(sL_2+R_2)} \tag{3-3}$$

$$Z_{oO}(s)=-\left.\frac{\hat{v}_{pcc}}{\hat{i}_o}\right|_{\hat{u}_f=0} =\frac{(sL_1+R_1)\cdot(\frac{1}{sC_f}+R_C)}{(sL_1+R_1)+(\frac{1}{sC_f}+R_C)}+(sL_2+R_2) \tag{3-4}$$

Therefore, the equivalent circuit of the LCL-type inverter can be depicted as Fig.3-6. The individual inverter can be regarded as a current source in parallel with the output

impedance because the current controlled feedback loop is applied in the closed-loop system. The whole circuit can be regarded as a current source, which is not ideal because of the existence of output impedance. $i_s(s)$ refers to the equivalent current source, which is expressed as (3-5). Z_{oC} denotes the closed-loop output impedance of the inverter, which is expressed as (3-6):

$$\hat{i}_s(s) = \frac{T_i(s)}{1+T_i(s)} \cdot \frac{\hat{i}_{ref}(s)}{H_s(s)} - \frac{1}{Z_{oC}(s)} \cdot \hat{v}_{pcc}(s) \tag{3-5}$$

$$Z_{oC}(s) = -\frac{\hat{v}_{pcc}}{\hat{i}_o}\bigg|_{\hat{u}_f=0} = Z_{oO}(s) \cdot [1+T_i(s)] \tag{3-6}$$

According to (3-5), the expression can be derived by Fig.3-3. Therefore, the output current certainly contains two components. Based on the equations above, the equivalent circuit of the LCL-type inverter can be derived as Fig.3-6.

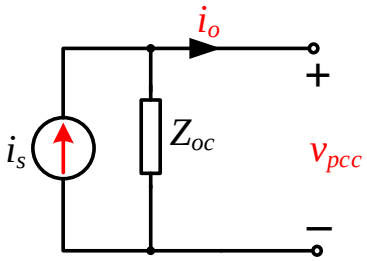

Fig. 3-6. Equivalent circuit of LCL-type inverter

3.1.2 Inverter with Weak Grid

Generally, a large and stiff power grid can be regarded as an ideal voltage source; the output impedance can be regarded as zero. However, a weak grid is not, and the grid impedance cannot be ignored. According to (3-5), the existence of Z_{oC} affects output current because the current is relative to the voltage harmonics. The equivalent circuit of the inverter is the same as Fig.3-6.

To verify the effect of large impedance in a weak grid, a tested system, including a grid-

connected inverter, weak grid and a simple feedback control loop, is provided in this section. The parameters are shown in Table.1.

Table 1. Parameters of GCI with weak grid

Description	Parameters	Value
Inverter side inductance of LCL filter	L_1	7.2 mH
Series resistor of the capacitor	R_c	10 Ω
The capacitor of LCL filter	C_f	6 μF
DC-link voltage	V_{dc}	405 V
Grid side inductance	L_g	3 mH
Grid side inductance of LCL filter	L_2	1.2 mH
Carrier wave frequency	f_{cr}	10 kHz
Sampling frequency	f_s	20 kHz
Triangle wave magnitude	V_{tri}	199 V
Output Power	P_o	4kW
Feedback Coefficient	H_s	0.55
Fundamental frequency	f_1	50 Hz
Proportional gain	K_p	35
Integral gain	K_i	60000

3.2 Impedance-Based Stability Criterion

3.2.1 Introduction

When the grid-connected inverter is connected with a weak grid in which the grid impedance cannot be ignored, the common approaches to analyze the stability of GCI

with weak grid require the specific inverter control models with high grid impedance, which is difficult to summarize.

Through the discussion above, we must theorize a general criterion to analyze the stability and therefore address the instability problem caused by weak grid conditions. In most cases, the impedance-based stability criterion is an effective and practical way for the whole grid system. Most importantly, this stability criterion can be applied to variable grid conditions when grid impedance changes. Besides, the criterion requires only an external model of the inverter, which is much easier to obtain[8].

3.2.2 Theoretical Derivation

Fig.3-7 denotes the equivalent circuit of the case that GCI series connected with a weak grid. As seen, Z_{oC}(s) is equal to the impedance of the inverter side. Z_g(s) denotes the equivalent grid impedance. Therefore, the grid model can be simplified as an individual current source connected with the non-ideal load. The impedance-based stability criterion is derived from two underlying assumptions.

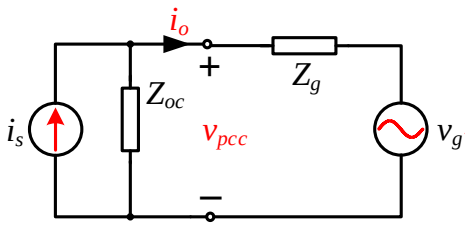

Fig. 3-7. A non-ideal current source with a non-ideal voltage source

To begin with, the small-signal representation of the grid system, which is shown in Fig.3-7, is required to simplify the model with linear representation. Based on the linear model, the output current of the inverter can be expressed as:

$$i_o(s) = i_s(s) \cdot \frac{Z_{oC}(s)}{Z_g(s) + Z_{oC}(s)} - v_g(s) \cdot \frac{1}{Z_g(s) + Z_{oC}(s)} \tag{3-7}$$

The voltage of point of common coupling can be expressed as v_{pcc}:

$$v_{pcc}(s) = v_g(s) \cdot \frac{Z_{oC}(s)}{Z_g(s) + Z_{oC}(s)} + i_s(s) \cdot \frac{Z_g(s) \cdot Z_{oC}(s)}{Z_g(s) + Z_{oC}(s)} \tag{3-8}$$

The first assumption is that the current source itself (inverter) can be assumed stable when unloaded. Firstly, if the inverter cannot be an ideal current source, the impedance of the inverter side cannot be ignored. The equivalent circuit of the first assumption is shown as Fig.3-8. According to Fig.3-8, when the inverter unloaded, only the current will be affected because of the grid voltage source.

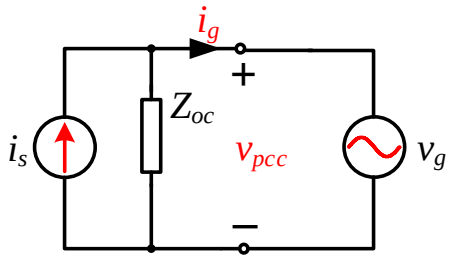

Fig. 3-8. A non-ideal current source unloaded

The output components i_o and v_{pcc} can be expressed as (3-9) and (3-10):

$$i_g(s) = i_s(s) - \frac{1}{Z_{oC}(s)} \cdot v_{pcc}(s) \rightarrow i_g(s) \text{ is stable} \tag{3-9}$$

$$v_{pcc}(s) = v_g(s) \rightarrow \quad v_{pcc}(s) \text{ is stable} \tag{3-10}$$

In this case, therefore, two requirements need to be satisfied to make the inverter operate stably as an individual part. Firstly, $1/Z_{oC}(s)$ should be stable to meet (3-9). Secondly, $v_g(s)$ should be stable to meet (3-10).

The second assumption is that the load can be assumed stable when supplied by an ideal current source. In this case, the output impedance can be ignored because the current source (the inverter) is ideal, and the grid impedance is introduced in the equivalent circuit. The grid side is regarded as a weak grid condition.

The equivalent circuit of the second assumption is shown as Fig.3-9. According to Fig.3-9, when the inverter unloaded, only the current will be affected because of the grid voltage source.

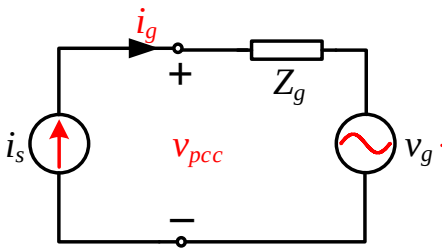

Fig. 3-9. An ideal source with a non-ideal voltage source

The output components i_o and v_{pcc} can be expressed as (3-11) and (3-12):

$$i_g(s) = i_s(s) \rightarrow i_g(s) \text{ is stable} \tag{3-11}$$

$$v_{pcc}(s) = v_g(s) + i_s(s) \cdot Z_g(s) \rightarrow v_{pcc}(s) \text{ is stable} \tag{3-12}$$

Seemingly, two requirements need to be satisfied to let the grid operate stably as an individual part. Firstly, $i_g(s)$ should be stable to meet (3-11). Secondly, $Z_g(s)$ should be stable to meet (3-12).

After reviewing these two underlying assumptions, the original model can be simplified based on them. According to (3-7) and (3-8), these two equations can be rearranged as (3-13) and (3-14):

$$i_o(s) = \left(i_s(s) - v_g(s) \cdot \frac{1}{Z_{oC}(s)} \right) \cdot \frac{1}{1 + \dfrac{Z_g(s)}{Z_{oC}(s)}} \tag{3-13}$$

$$v_{pcc}(s) = \left[v_g(s) + i_s(s) \cdot Z_g(s) \right] \cdot \frac{1}{1 + \dfrac{Z_g(s)}{Z_{oC}(s)}} \tag{3-14}$$

$$T_m(s) = \frac{Z_g(s)}{Z_{oC}(s)} \tag{3-15}$$

Basing on the assumptions above, the left-hand parts of the expressions of output components are assumed to be stable. Both of the right-hand parts of output components is the open-loop transfer function of a simple feedback control loop whose loop gain of the equivalent circuit is $T_m(s)$.

According to the equation (3-15), the loop gain $T_m(s)$ is $Z_g(s)/Z_{oC}(s)$. Therefore, the grid-connected inverter with a weak grid is stable only if $Z_g(s)/Z_{oC}(s)$ (the ratio of the grid impedance to the inverter output impedance) satisfies the Nyquist criterion.

The introduction of impedance-based stability criterion indeed helps with the design of the control loop. Therefore, the goal of the control loop design should be made to match inverter output impedance or grid side impedance with each other to meet the Nyquist criterion. If not, then the control method should be improved.

3.3 The theoretical function of the SAS

In [49], APF is proved to be able to handle the harmonic problems by compensating for harmonic components. However, it will still bring resonance and instability problems to GCI. The traditional active power filter is not enough for improving the performance of the inverter.

However, designing a GCI with optimal parameters to adapt to the varying grid condition is not practical to implement. Therefore, the series-connected adaptive stabilizer (SAS) model is proposed to adaptively deal with these issues when the grid condition is changing. This improving shaping scheme is similar to the active damping method while it shapes the grid side impedance.

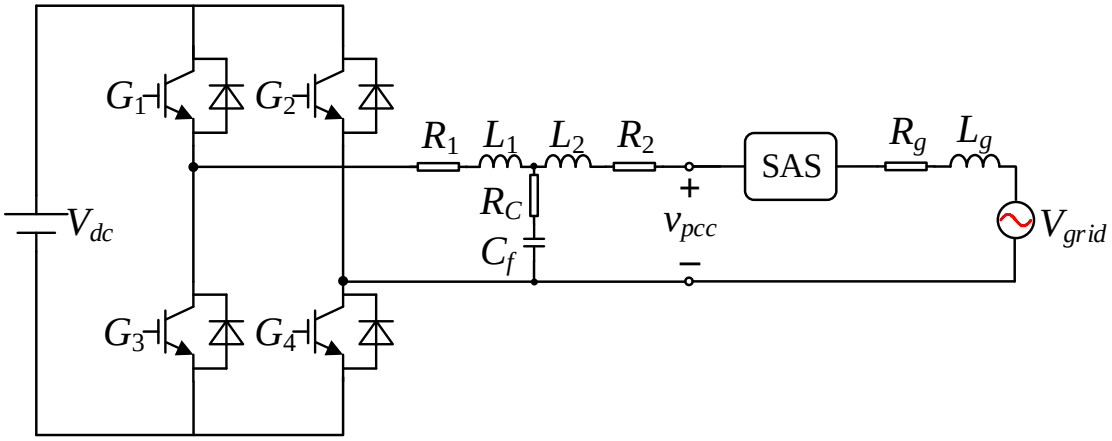

Fig. 3-10. Position of the SAS model

As shown in Fig.3-10, the proposed series-connected adaptive stabilizer (SAS) is in series with the GCI and the grid impedance. It treats the GCI as a black box and does not need to know any internal information or parameters of the GCI. The SAS model devotes itself to shaping the grid impedance via adding a series impedance Z_{SAS} to the first grid impedance.

Therefore, the Bode plot of introducing the proposed improving method is provided to indicate the function of it is the ideal case. The designed model consists of the following functions: The introduction of it will improve the performance and stability of GCI with a weak grid at around the crossover frequency. Besides, the proposed model should not affect the whole system at the rest of the frequency range.

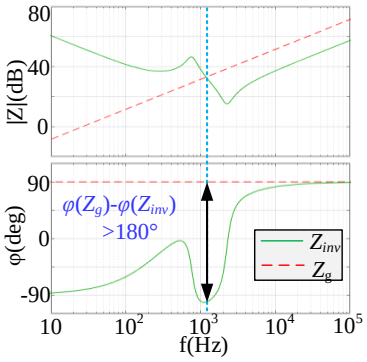

(a)

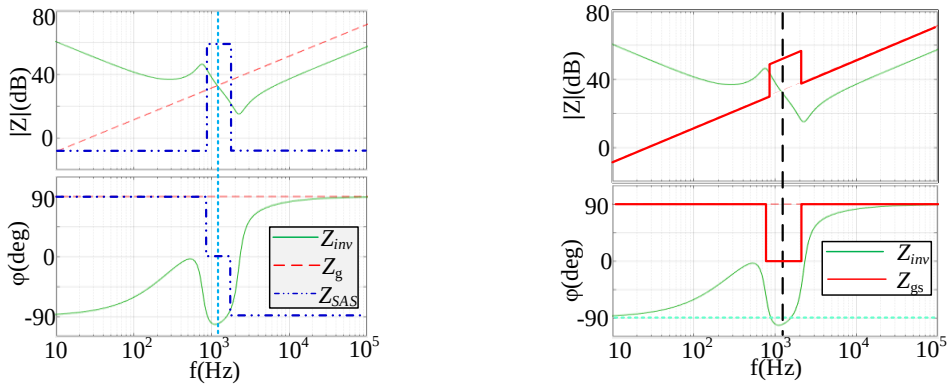

(b) (c)

Fig. 3-11. (a)Original bode plot of Z_g and Z_{inv}; (b)The ideal bode plot of Z_{SAS}; (c)Bode plot of shaped grid impedance

As shown in Fig.3-11, it is presented that the function of SAS in the ideal case is almost equivalent to the theoretical analysis. Firstly, the Bode plot of the original system (inverter with a weak grid without SAS model) is depicted as Fig.3-11(a). Before introducing SAS, $|Z_g(s)|$ is intersected with $|Z_{inv}(s)|$ at the intersection frequency f_{int}, and $\varphi(Z_g)$-$\varphi(Z_{inv})$ is larger than 180° at intersection frequency f_{int}. That is to say; the system is unstable because the phase difference between the grid impedance and output impedance of the inverter at the intersect frequency is larger than 180 degrees.

The blue curve in Fig. 3-11(b) indicates the Bode plot of the SAS model in the ideal case. As seen, it has basically two features that are consistent with what is discussed previously. The equivalent impedance of the SAS model refers to Z_{SAS} and it is in series with both the inverter and utility grid. Z_{SAS} performs as a very large resistor characteristic ($|Z_{SAS}|>>|Z_g(s)|$) around f_{int} where $\varphi(Z_g)$-$\varphi(Z_{inv})$>180°(the unstable area). Besides, $|Z_{SAS}|$ (magnitude of Z_{SAS}) is very small at the other frequency range. Thus the introduction of it will not affect any performance at the rest frequency range.

According to Fig. 3-11(c), the Bode plot of the system after shaping the impedance is shown to verify the correctness of it under the ideal case. Since the SAS model is in series with the grid side, the grid impedance will be shaped to Z_{gs}:

$$Z_{gs}(s) = Z_g(s) + Z_{SAS} \tag{3-16}$$

Through the Bode plot, the red curve, which is equivalent to the overall impedance, indicates that the shaped grid impedance will not lead to instability issues because the phase difference can be suppressed under the limit. According to the above discussion, in the ideal case, the introduction of SAS can improve the phase margin of the system and improve the stability of GCI with a weak grid.

3.4 Topology and control block of proposed SAS

As mentioned in the previous introduction, the underlying topology is almost the same as the active power filter. However, unlike the traditional series active power filter, the proposed SAS model adopts the new adaptive control method to achieve the ideal function for stability improvement. The difference between the control method in SAS and series APF will be discussed as well.

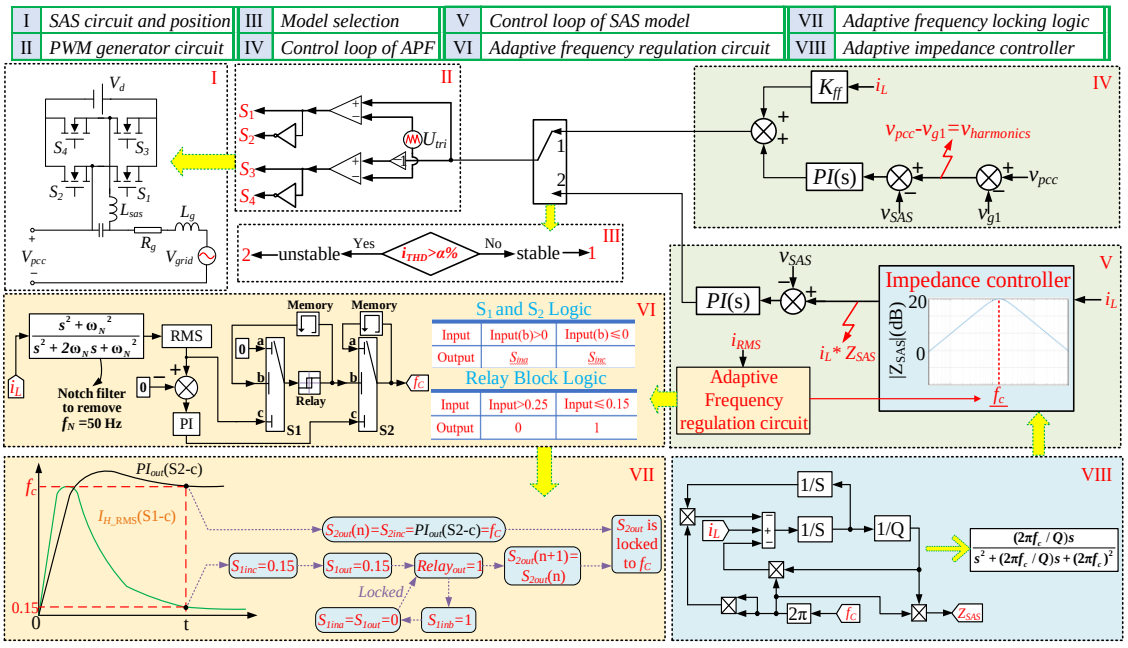

Fig. 3-12. Topology and control block of the SAS model

As shown in Fig.4-3, the topology and position of the SAS model is indicated in Model I. Besides, and the whole figure consists of a control block and its logic block to achieve

it. In order to clarify the function and control method of the proposed SAS, the whole block at the grid side is divided into several subsystems, and the inverter side is ignored. The individual content block will be introduced as follows.

The proposed system consists of a Series Active Power Filter(SAPF) with two different control schemes. The first one is the conventional control method. The other one is the proposed SAS control scheme, including an adaptive frequency regulation circuit with an impedance controller. The control scheme is selected through a model selection block.

3.4.1 Block I: SAS topology and position

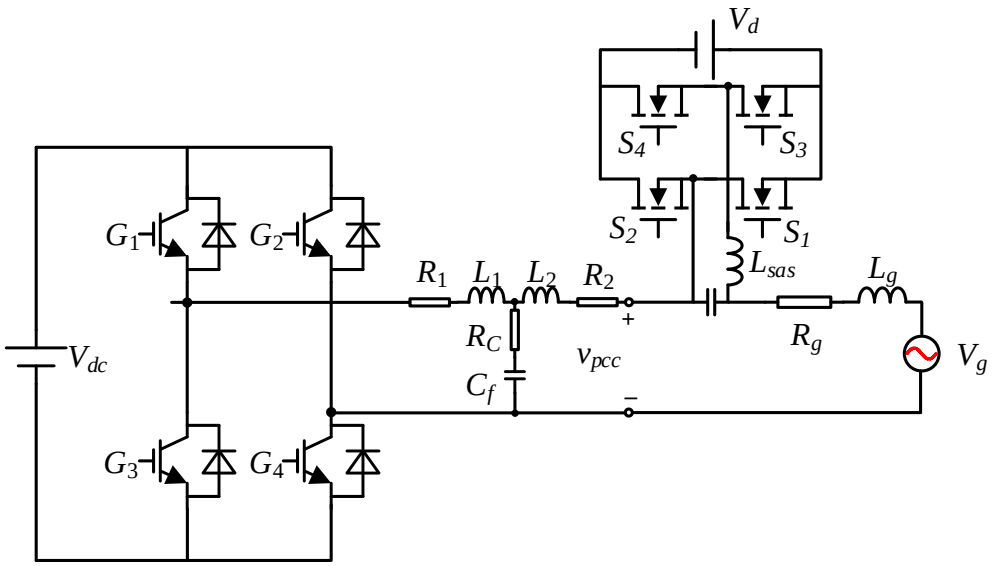

Fig. 3-13. The physical model and position of SAS

Fig.3-13 (Block I) depicts the topology and position of SAS. Generally, the entire physical topology of SAS is the same as a series active power filter (APF). The gate signals are generated by the control loop, which depends on the characteristics of the whole system. Both APF and SAS can make the original model act as equivalent impedance in series with grid impedance.

However, the proposed SAS model has a different control method comparing with

traditional APF control method. The only difference is that the SAS model will generate an adaptive impedance to match the condition. That is the main difference between APF and SAS, which can achieve the proposed function that traditional series APF cannot handle.

3.4.2 Block II: PWM generation circuit

Before introducing the control block, the PWM technology is applied to generate four gate signals for the active power filter. In this case, unipolar PWM technology is used in the circuit. Fig.4-5 depicts the unipolar PWM generation circuit.

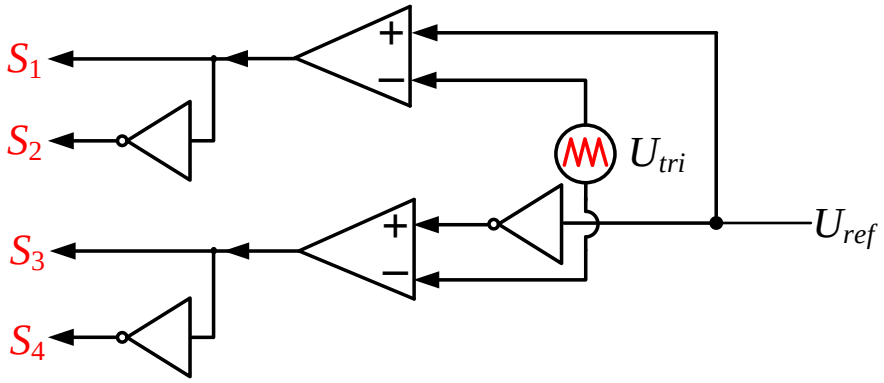

Fig. 3-14. Unipolar PWM generation circuit

As shown in Fig.3-14, U_{tri} denotes the carrier wave and U_{ref} denotes the reference wave. The unipolar modulation normally requires two sinusoidal modulating waves U_{ref} and U_{ref-} which are of the same magnitude and frequency, but the phase difference is 180 degrees [76].

After being compared with a common triangular carrier wave U_{tri}, these two modulating waves conduct two gating signals S_1 and S_3 for the two switches in active power filter, S1, and S3, respectively.

It is indicated that S1 and S3 do not switch at the same time. However, in the bipolar

PWM, all four power devices are switching simultaneously. This is the main difference between bipolar PWM and unipolar PWM. Therefore, when choosing the PWM technology, the unipolar PWM has the advantage of less switching losses. Although it is harder to implement than the bipolar PWM, the harmonic performance is much better than it[18].

3.4.3 Block III: Model Selection

As an adaptive impedance shaping method, the SAS model includes two working modes: Traditional APF mode and the proposed SAS mode. That is to say, the mode will be switched automatically when the characteristics or certain parameters satisfy the criterion.

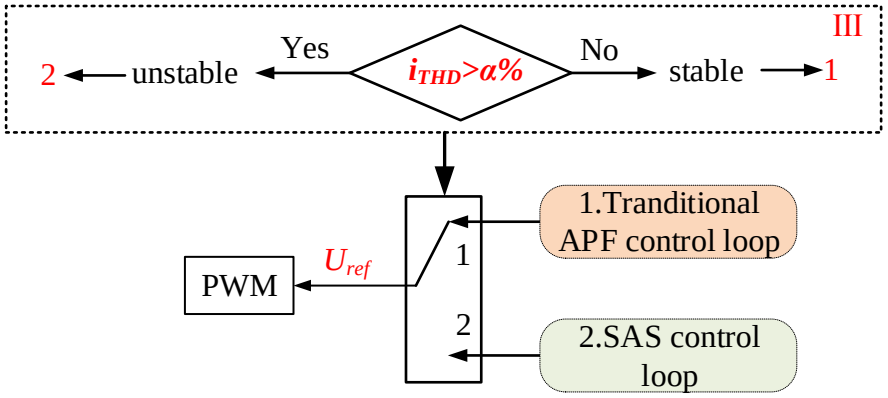

Fig. 3-15. Model selection of SAS

As shown in Fig.3-15 (Block III), the control block can switch between APF mode and SAS mode automatically. The switching criterion is set as follows: (α=6 in this case study). If the THD value of output current is less than α percent, the system will be switched into the first control loop, which adopts traditional APF control loop.

However, when the THD value of output current is more than α percent, the system will be switched into the proposed SAS control loop.

Therefore, when THD of the output current surpasses the limited value, the system will

be identified as requiring to be improved because of the instability issue. In this case, the control loop will be switched into the SAS control loop.

Moreover, when THD of the output current does not reach the limited value, the control loop will be unchanged as a series active power filter.

Thus, the active power filter adopts the SAS control loop to address the instability issues. After the stability of the system is improved without a severe instability issue, the system will apply APF control loop automatically to ensure the power quality and harmonic performance. This adaptive mode makes the whole system cater to variable grid condition or inverter parameters.

3.4.4. Block IV: APF Control Loop

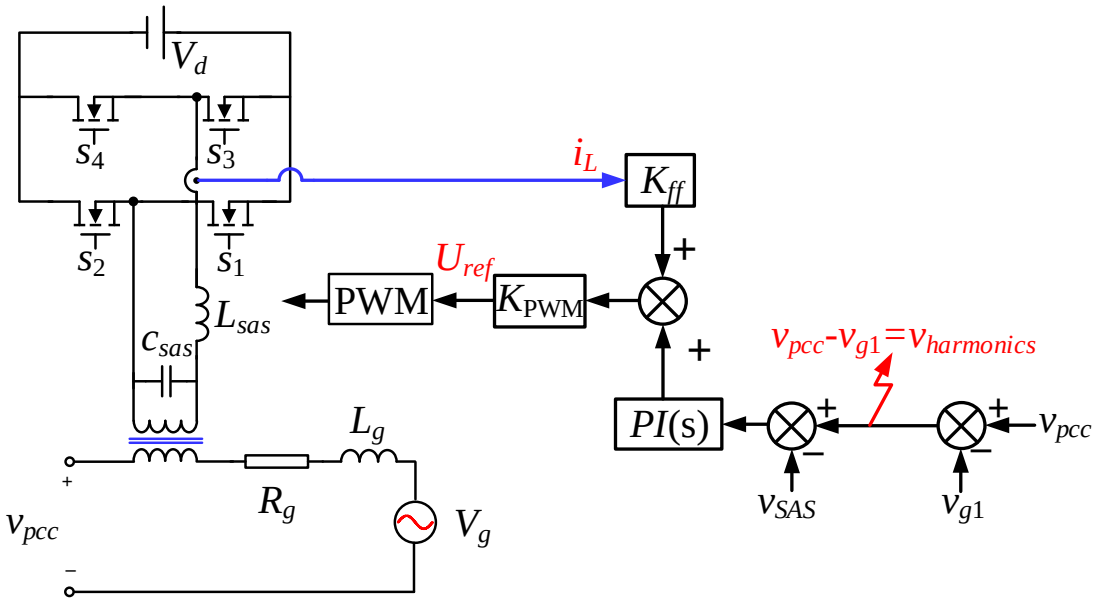

Fig. 3-16. The control loop of APF model

As mentioned before, series APF with traditional control loop mainly concentrate on the harmonics issues. When the system is switched into the APF control loop, the control loop is shown as Fig.3-16 (Subsystem IV) including a voltage-controlled feedback loop and a current-controlled feedforward loop.

As shown in Fig.3-16, i_L denotes the current of the SAS model. v_{pcc}, v_{sas} and v_{g1} refer to voltage of point of common coupling, the voltage of the SAS model, and fundamental grid voltage respectively. For the voltage-controlled feedback loop, the designed loop is required to eliminate the voltage harmonics. Therefore, the reference value is the voltage harmonics, which is expressed as (3-17):

$$v_{harmonics} = v_{pcc} - v_{g1} \tag{3-17}$$

The reference voltage signal of PWM generation circuit U_{ref} can be expressed as (3-18):

$$U_{ref} = K_{PWM} \cdot \mathrm{PI}(s) \cdot \left[v_{pcc} - v_{g1} - v_{SAS} \right] + i_L \cdot K_{ff} \tag{3-18}$$

From the expressions of output voltage reference value, it is indicated that the control loop contains the inner current loop and outer voltage loop. The error between voltage harmonics and output voltage of the SAS model goes through the PI controller in order to make the compensating voltage match the harmonics. Therefore, the unbalanced voltage can be corrected.

When applied in the tested system, equivalent series resistor(ESR) R_{sas} may be adopted in the topology of the active power filter. The parameters are shown as Table 2. f_s denotes the sampling frequency, and f_{cr} denotes the carrier wave frequency.

Table 2. Parameters in APF control loop

Description	Parameters	Value
The inductance of the active power filter	L_{sas}	2mH
The resistor of the active power filter	R_{sas}	10 Ω
The capacitor of the active power filter	C_{sas}	12 μF

DC-link voltage	V_{dc}	100 V
Grid side inductance	L_g	3 mH
RMS value of grid voltage	V_g	220 V
Carrier wave frequency	f_{cr}	10 kHz
Sampling frequency	f_s	20 *k*Hz
Feedforward coefficient	K_{ff}	1
Voltage proportional gain	K_{vp}	30 A/V
Voltage integral gain	K_{vi}	400 A/(V·s)
Fundamental frequency	f_1	50 Hz

3.4.5 Block V:SAS Control Loop

According to the impedance-based stability criterion, however, the system will be unstable in the weak grid condition. In this case, the traditional APF control loop may not handle the instability issues. Therefore, when the system is detected to be unstable, the control loop will automatically switch to SAS control mode, including an adaptive current controller, which is shown as Fig.3-17(Block V).

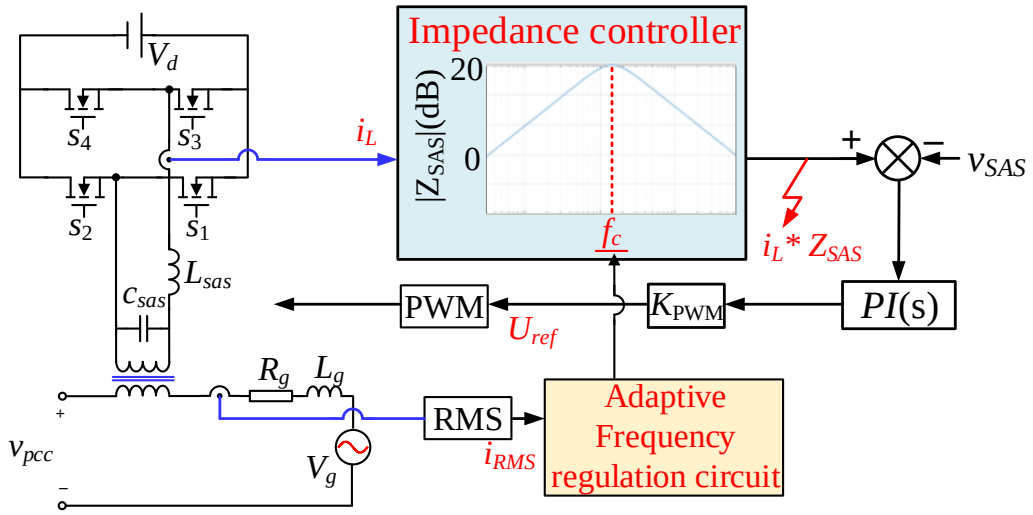

Fig. 3-17. The control loop of the SAS model

As for the SAS control loop, the goal of it is certainly relative to dealing with the instability issues in weak grid condition, which cannot be addressed with traditional APF

control loop.

According to the previous discussion of SAS function in the ideal case, the SAS model can improve the stability by increasing the phase margin in a designed frequency range, which can be detected by the regulation circuit.

Generally, the purpose of the proposed model is realized by adding a compensating impedance in series with the grid impedance. Therefore, the phase margin of the system is promised because of the existence of a series impedance after being shaped.

As shown in Fig.3-17, the control loop only contains a simple current controlled feedback loop. In the beginning, the root mean square (RMS) value of output current is imported into the adaptive frequency regulation circuit as the input value.

After the frequency regulation circuit receiving the RMS value, the whole circuit will generate corresponding frequency value, which is used as the center frequency(or crossover frequency) value to realize the proposed function of the SAS model.

After the crossover frequency being locked as a certain value, the impedance controller will apply the frequency value to generate an equivalent impedance. This is the function of the impedance controller. Therefore, the frequency regulation circuit is designed to be similar to a band-pass filter in order to realize the previous improvement.

The output signal, which is equal to reference wave U_{ref} can be expressed as (3-19):

$$U_{ref} = \mathrm{PI}(s) \cdot (i_L \cdot Z_{SAS}) \tag{3-19}$$

$$\mathrm{PI}(s) = K_{\mathrm{vp}} + \frac{K_{\mathrm{vi}}}{s} \tag{3-20}$$

The parameters of the active power filter and PI controller are shown as Table. 3.

Table 3. Parameters in SAS control loop

Description	Parameters	Value
The inductance of active power filter	L_{sas}	2mH
The resistor of active power filter	R_{sas}	10 Ω
The capacitor of active power filter	C_{sas}	12 μF
DC-link voltage	V_{dc}	100 V
Grid side inductance	L_g	6 mH
RMS value of grid voltage	V_g	220 V
Carrier wave frequency	f_{cr}	10 kHz
Sampling frequency	f_s	20 kHz
Feedforward coefficient	K_{ff}	1
Voltage proportional gain	K_{vp}	30 A/V
Voltage integral gain	K_{vi}	400 A/(V·s)
Fundamental frequency	f_1	50 Hz

3.4.6 Block VI &VII: Adaptive Frequency Regulation Circuit

After introducing the function and basic working procedure of SAS control loop, the prominent parts of the SAS model need to be deeply investigated.

In Fig.3-18 (Block VI), an adaptive frequency regulation circuit is further presented. As shown in Block VI, i_L (current going through L_{SAS}) firstly goes through a notch filter which can remove the fundamental current (f_1=50Hz) and derives current harmonics i_h.

The expression of the transfer function of the notch filter is shown as (3-21). Then, the root mean square(RMS) value of i_h is obtained through an RMS block and goes to input C port of the first switch S1.

$$NF(s) = \frac{s^2 + \omega_N{}^2}{s^2 + 2\omega_N s + \omega_N{}^2} \tag{3-21}$$

$$\omega_N = 2\pi \cdot f_N \tag{3-22}$$

In the tested system, notch filter requires removing the fundamental frequency components. Therefore, the value of N in both (3-21) and (3-22) is designed as 1.

Moreover, i_{h_RMS} is compared with 0, and the error between them will be sent to the proportional-integral(PI) controller. The output value of the PI controller is used as the input value at *c* port of the second switch S2.

The switch block passes through the first input or the third input based on the value of the second input(*b* port). The first and third inputs are denoted as data inputs. The second input is called the control input. Specify the condition under which the block passes the first input by using the criteria for passing the first input and threshold parameters. Therefore, according to the logic chart in Fig.3-18, the threshold value of the first switch is zero. That is to say, when the value of port *b* is positive, the output of the switch is equivalent to the value at the port *a*. On the other hand, when the value of port *b* is negative, the output of the switch is equivalent to the value at port *c*. Similarly, the threshold value of the second switch S2 is zero as well.

Besides, the logic block contains two Memory blocks and two Relay blocks to achieve a certain function by combination. The Memory block holds and delays its input by one major integration time step. When placed in an iterator subsystem, it holds and delays its input by one iteration. This block accepts continuous and discrete signals. The block accepts one input and generates one output. Each signal can be scalar or vector. If the input is a vector, the block holds and delays all elements of the vector by the same time step. Therefore, the control inputs of the two switches are the output value of the Relay block with one-time step difference.

With regard to the Relay block, the Relay block allows its output to switch between two specified values. When the relay block is on, it remains on until the input drops below the value of the switch-off point parameter. When the relay is off, it remains off until the input exceeds the value of the switch on point parameter. The block accepts one input and generates one output.

The Switch on point value must be greater than or equal to the Switch off point. Specifying a switch on point value greater than the Switch off point models hysteresis, whereas specifying equal values models a switch with a threshold at that value.

According to Fig. 3-18, the switch on point value is 0.25, while the switch-off point value is 0.15. Unlike common relay block design, the relay block in the tested system has different characteristics. It output 0 when the block is on and output 1 when the block is off.

Finally, the output frequency value f_c will increase aiming to improve the stability of the system because of the existence of i_{h_RMS}. The expression of PI controller is shown as (3-23):

$$\mathrm{PI}(s)=K_{\mathrm{cp}}+\frac{K_{\mathrm{ci}}}{s} \tag{3-23}$$

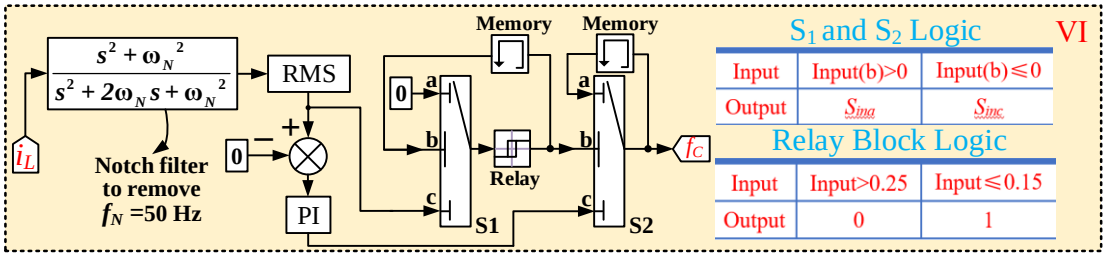

Fig. 3-18. Adaptive frequency regulation circuit

After introducing the individual block in the frequency regulation circuit, the frequency locking procedure needs to be specified.

At the very beginning, the original control input is zero so that the output of two switches

are the value at port *c* of two switches, respectively. The output frequency value is generated and then transported to the impedance controller. After applying the series impedance in the system, the current and other output components will get changed and then feedback to the regulation circuit. Since the error between i_{h_RMS} and reference value still exists, the output value of the PI controller will get increased due to the existence of severe current harmonics.

When the output is corrected as the desired center frequency, which means the impedance controller can stabilize the system at this right frequency value. In this case, the current harmonics are suppressed as the desired value. Meanwhile, i_{h_RMS} is less than 0.15. At this moment, according to locking logic, as shown in Fig.3-19(Block VII), the whole locking process can be expressed as follows:

(1) Locking of S_1 and Relay block

input port *c* of $S_1 \leq 0.15 \rightarrow$input of Relay block$\leq 0.15 \rightarrow$output of Relay block is 1$\rightarrow$the input port *b* of S_1 is 0$\rightarrow$the output of Relay block is always 1. Therefore, the first switch and the relay block are locked.

(2) Locking of S_2 and f_c

the output of Relay block is always 1$\rightarrow$the input port *b* of S_2 is 1$\rightarrow$the output of S_2 is $f_c \rightarrow$the input port *a* of S_2 is $f_c \rightarrow$the output of S_2 is always locked as f_c.

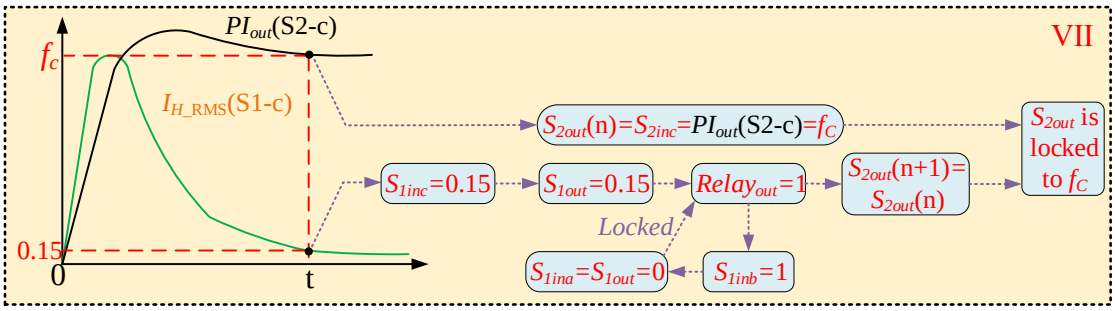

Fig. 3-19. Locking logic of adaptive frequency regulation circuit

In summary, according to the locking logic, the frequency value will be locked only if the output value of the PI controller generates a proper frequency value for the impedance controller. However, the output value of the PI controller is still increasing as the existence of the error. Therefore, the introduction of the Memory block is prominent and indispensable for the output of correct value.

After one sampling period(one time step), the parameters and feedback variables are updated. In this case, the system is stabilized. The memory block can output the frequency value one-time step before. At the same time, the two switches and the relay block are locked as a certain output value. Thus, the application of the Memory block prevents the trouble of missing the correct value.

3.4.7 Subsystem VIII: Adaptive impedance controller

The output of the frequency regulation circuit is locked as the right frequency value f_c. Thus, the output impedance of the SAS model is locked as well. After the adaptive frequency regulation circuit being locked, the impedance controller will utilize the frequency value imported into the block to make the block as a band-pass filter. The impedance controller is designed as Fig.3-20.

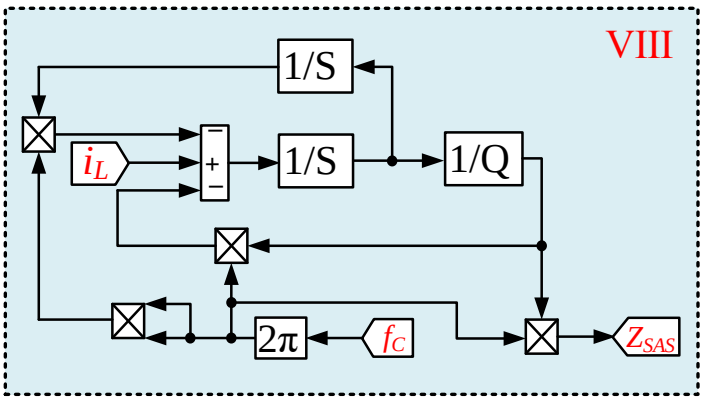

Fig. 3-20. Block diagram of the adaptive impedance controller

Fig.3-20 presents the block diagram of the adaptive impedance controller. The output of

frequency regulation circuit will be applied as the input value of the impedance controller shown as Fig.3-20 (Block VIII).

$$Z_{SAS} = \frac{(2\pi f_c / Q)s}{s^2 + (2\pi f_c / Q)s + (2\pi f_c)^2} \tag{3-24}$$

The whole loop transfer function is shown as (3-24) which is equivalent to a band-pass filter whose center frequency value is f_c. Therefore, the characteristic of the impedance controller is similar to the bandpass filter. As known, the bandpass filter allows the components between two different frequencies to pass. Combining with the designed goal of the SAS model, the requirement is that the proposed SAS model can improve the phase margin at the frequency range that the phase difference surpasses 180 degrees. Besides, it is required that the SAS works at this certain range without influencing other frequency ranges.

Therefore, the impedance controller, which needs to be realized in series with utility grid, should adopt a bandpass filter for improvement.

It has a large amplitude around center frequency automatically detected in Block VI and a very low amplitude at other frequency ranges. Thus, the proposed control loop can improve the original system stability around f_c without affecting the characteristics of the system at the left frequency range.

The output value refers to the equivalent output impedance of the SAS model Z_{SAS}. It acts as a series-connected impedance with the weak grid. Thus, the grid impedance is shaped through the introduction of the SAS model.

The prominent parameter in the impedance controller is the value of Q. Q, in this block diagram, represents the quality factor. For a band pass filter, the quality factor is the ratio of the center frequency of the bandpass over the entire bandpass region from the lower to upper cutoff frequencies. That is to say, the value of Q reflects the width of the pass

band[52].

For given band-pass circuit design, the value of Q gives a good measure of whether the band-pass is narrow or wide. A high-quality factor indicates the passband is narrow. That is to say, the effective range of the impedance controller is narrow if the quality factor is high.

As for the whole tested system; if the range is narrow, the detected frequency value should be much more accurate to ensure the desired function. However, the sampling frequency should be high enough to provide an accurate frequency value, and this case is not practical.

Therefore, a low-quality factor is always preferred. A low-quality factor indicates the bandpass is wide. Certain bandpass filter designs only allow for narrowband band-passes or high Q-factors. Others allow for much more full band passes, or low Q-factors.

In the tested system, we only need a low Q-factor to ensure a wide band-passes. Therefore, the value of Q is designed as 0.5 in this case study.

3.5 Experiment verification

The stability of GCI with the SAS model under a weak grid will be experimentally investigated in this section. Moreover, the effectiveness of the proposed modified SAS model for system stability enhancement and the original APF model for system harmonics suppression will also be verified, respectively. Subsequently, the proposed SAS control scheme will be summarized in various grid conditions.

As discussed in the previous section, the SAS model is series-connected with both grid voltage source and the grid-connected inverter. The main circuit of the system is depicted in Fig.3-21.

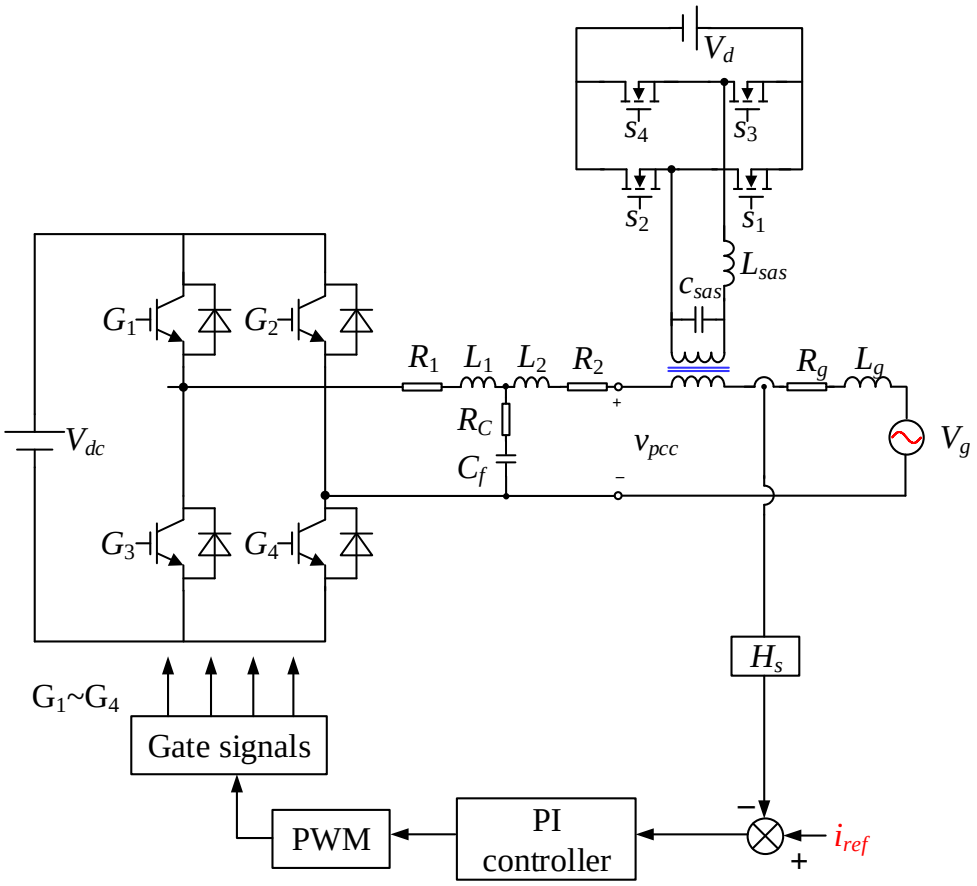

Fig. 3-21. GCI with SAS model under weak grid

The parameters in the control loop of the SAS model are shown as Table.2. The system parameters of the GCI are shown in Table.3.

Description	Parameters	Value
The inductance of the active power filter	L_{sas}	$2m$H
The resistor of the active power filter	R_{sas}	10 Ω
The capacitor of the active power filter	C_{sas}	12 μF

DC-link voltage	V_{dc}	100 V
Grid side inductance	L_g	3 mH
RMS value of grid voltage	V_g	220 V
Carrier wave frequency	f_{cr}	10 kHz
Sampling frequency	f_s	20 *k*Hz
Quality factor	Q	0.5
Current proportional gain	K_{cp}	250 V/A
Current integral gain	K_{ci}	40000 V/(A·s)
Fundamental frequency	f_1	50 Hz
Voltage proportional gain	K_{vp}	30 A/V
Voltage integral gain	K_{vi}	200 A/(V·s)

3.5.1 SAS Model in Non-ideal Case

In this section, the function of the SAS model will be discussed in the tested system to verify the correctness of the proposed model. Furthermore, the function of the SAS model in the non-ideal case will be compared with that in the ideal case, which is discussed in the previous introduction.

As presented in the previous chapter, the impedance-based stability criterion is always used as a practical approach of analyzing the stability of the system. If the impedance ratio $Z_g(s)/Z_{oC}(s)$ satisfies the Nyquist criterion, the system is stable. Besides, the previous discussion predicts the bode plot of shaped grid impedance in the ideal case. It can promise a sufficient phase margin for the whole system.

As for the tested system, we need to verify if the impedance ratio of grid impedance to the inverter impedance, which is equivalent to loop gain $T_m(s)$, satisfies the Nyquist criterion. After introducing the series-connected model, the equivalent loop gain is changed as $T_{em}(s)$ because of shaped grid impedance:

$$T_{em}(s)=\frac{Z_{gs}(s)}{Z_{oC}(s)}=\frac{Z_g(s)+Z_{sas}(s)}{Z_{oC}(s)} \tag{4-8}$$

The Bode plot of the impedance ratio with SAS model is shown in Fig.3-22:

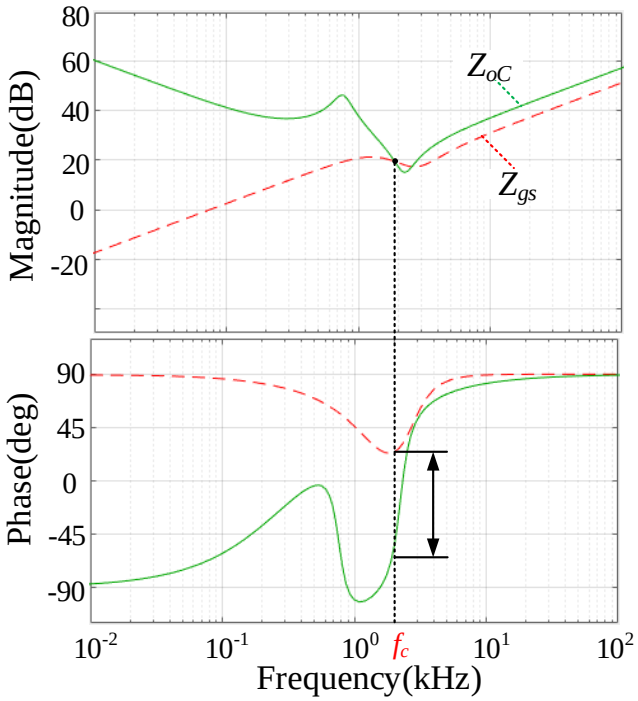

Fig. 3-22. Bode plot of the loop gain with the SAS model

As shown in Fig.3-22, the phase of equivalent grid impedance is attenuated because of the characteristic of the proposed SAS model. Although the curve of Z_{gs} and Z_{oC} still intersect with each other, the phase margin is improved. Specifically, without the SAS model, the system is unstable due to a negative phase margin. In the ideal case, the phase will be reduced by 90 degrees at the desired frequency range.

According to the Bode plot, as for the tested system, both the magnitude and phase are almost consistent with the previous prediction. As shown in Fig.3-22, the characteristic of equivalent grid impedance is similar to the resistor, and the magnitude of Z_{gs} is almost a constant at around the crossover frequency. Comparing with the original system, the magnitude of shaped grid impedance is increased in the ideal case. However, the introduction of the SAS model reduces the magnitude of grid impedance and demonstrate

resistive performance. Therefore, the phase difference between inverter side impedance and grid side impedance is no longer surpass 180 degrees. The phase margin in the system with the SAS model is positive. Besides, as shown in Fig.4-12, the characteristics of the system are almost not affected by the introduction of the SAS model.

3.5.2 Experimental verification

In order to verify the correctness of the proposed SAS model, the traditional APF and SAS model is tested in series with the LCL type inverter and different grid conditions. The experimental results will be presented to analyze whether the proposed SAS model is effective or not.

Fig.3-23 shows the performance testing results of introducing APF control method when GCI with weak grid condition which is detected as stable (grid inductor, in this case, is 1mH).

In the beginning, the steady-state waveform of grid-connected inverter with traditional active power filter under weak grid is demonstrated as Fig.3-23(b) and Fig.3-23(c). In the steady-state, the voltage of point of common coupling v_{pcc}, output current i_o, and voltage across the topology of active power filter(SAS model) v_{sas} are presented through three different channels. In Fig.3-23(d), THD of current is 3.17% when the current reference value is 5 A. When it jumps to 10 A, the THD value is less than before.

Fig.3-23(a) demonstrates the dynamic performance of the GCI with a traditional APF control loop. When the reference value jumps from 5 A to 10 A, the traditional APF can handle that varying conditions. Therefore, it is indicated that the traditional active power filter has the great dynamic performance.

Therefore, according to Fig.3-23, the traditional active power filter can maintain the stability of the GCI with a weak grid and suppress harmonics when the system is

stable(the grid impedance is low).

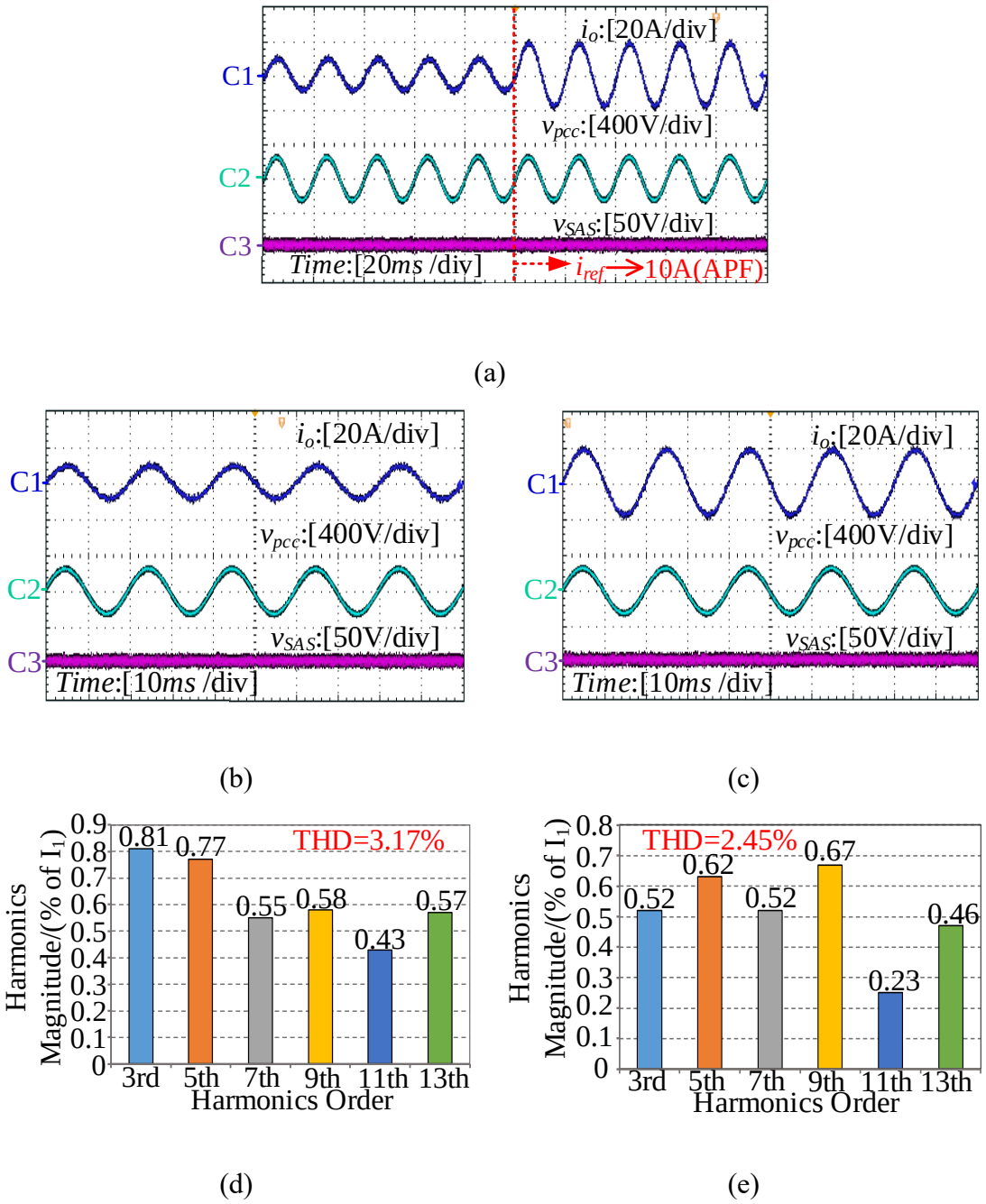

Fig. 3-23. The experimental result of the traditional APF: a) Stable system with APF when I_{ref} stepping from 5A to 10A; b) Stable system with APF when I_{ref}=5A; c) Stable system with APF when I_{ref}=10A; d) THD of current when I_{ref}=5A(stable); e) THD of current when I_{ref}=10A(stable).

Fig.3-24 shows the performance testing results of introducing APF control method when GCI under weak grid condition which is detected as an unstable system (grid inductor is increased to 6mH).

Obviously, in Fig.3-24(b), both current and voltage show many ripples. Besides, the output voltage of the active power filter begins to oscillate because of high grid impedance in weak grid conditions. In this case, the experimental results indicate that the outer voltage control loop cannot work effectively because even the voltage across the SAS has severe oscillation. The oscillations in the output current and voltage of PCC indicate that the system is unstable in this case.

According to Fig.3-24(a), the series active power filter(SAPF) with the traditional control loop even leads to more severe instability issues in weak grid conditions which is also shown as Fig.3-24(b). Thus, although the traditional APF method can handle the harmonic issues when the system is stable, it is not a practical way of improving stability in the weak grid condition (high grid impedance). Inversely, APF will deteriorate the instability issue in this case.

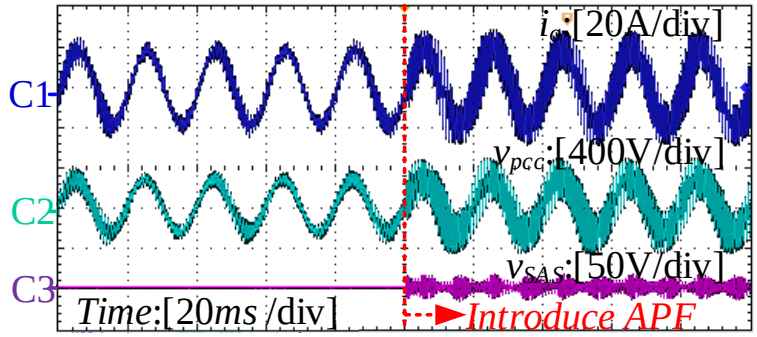

(a)

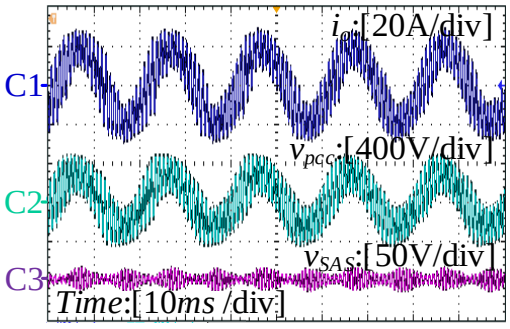

(b)

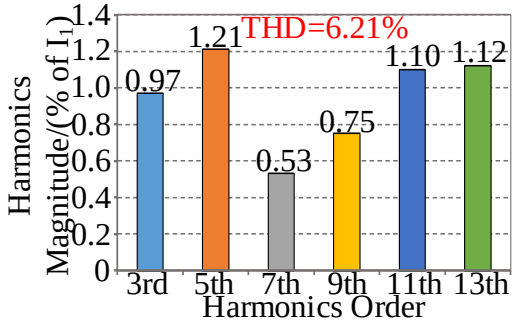

(c)

Fig. 3-24. The experimental result of the traditional APF (unstable system): a) Unstable system introducing APF at 0.5s Unstable system with APF; b) Unstable system with APF; c) THD of current with APF(unstable).

According to the experimental waveforms in Fig.3-24, the traditional APF should not be used as the series active power filter. The current harmonics cannot be attenuated by traditional active power filter. Moreover, the instability issue is amplified. Since the THD value surpasses the limited value, the control loop is selected as the SAS control loop. Therefore, the system will apply the SAS model in this case(weak grid condition) automatically, which is discussed in the previous introduction.

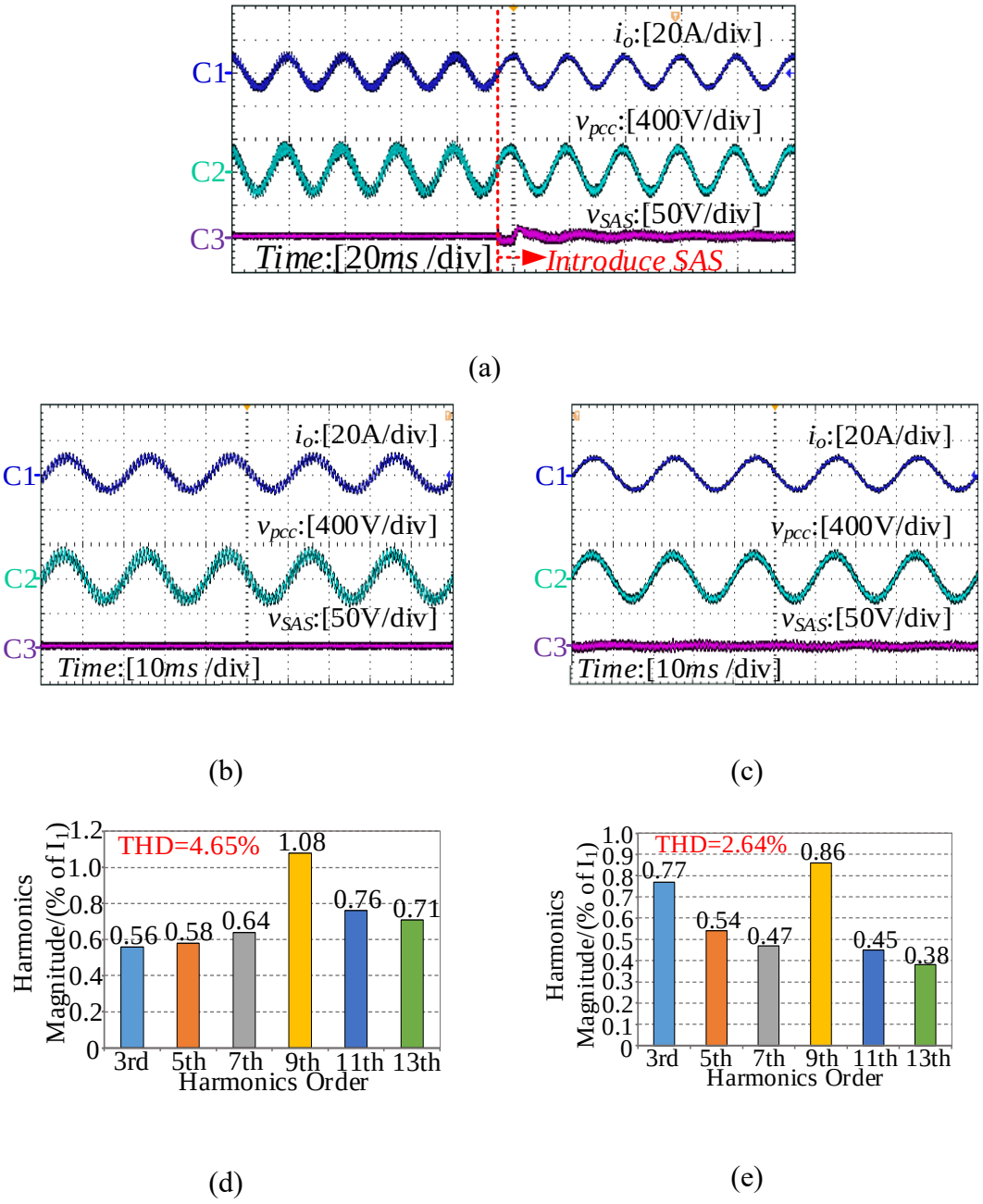

Fig. 3-25. The experimental result of the proposed SAS: a) Unstable system introducing SAS at 0.5s; b) Unstable system without SAS; c) Unstable system with SAS; d) THD of current without SAS(unstable); e) THD of current with SAS(unstable).

The experimental results of grid-connected inverter without the proposed SAS control method, with the SAS control method and introducing SAS control method during system running process(which reflects the dynamic performance of the SAS model) are displayed as Fig.3-25.

In Fig.3-25(a), the GCI with a weak grid is unstable and shows more ripples in the waveform of i_o and v_{pcc} without the SAS control strategy. As shown in Fig.3-25(b) and Fig.3-25(c), the original system and the system with the proposed SAS model are compared. The steady-state waveform of grid-connected inverter with active power filter under weak grid is demonstrated. The voltage of point of common coupling v_{pcc}, output current i_o, and voltage across the topology of SAS model v_{sas} are presented through three different channels. In the original system, the SAS model is not applied in the whole system and is regarded as a short circuit. In the improving system with the SAS model, the output current shows fewer harmonics. However, it still needs time to detect the frequency value and lock the SAS control loop. Fig.3-25(a) shows the dynamic waveform of introducing the SAS control method in the original system.

In order to achieve the SAS control loop, OPAL-RT 4500 and dSPACE 1007 are both used to realize the proposed scheme.

For the analog part, the model of the inverter with the power grid is achieved in the OPAL-RT 4500. OPAL-RT acts like a real-time simulator. It can process the physical model and output the desired voltage, current or other parameters as analog signals. Besides, the real analog signal is not the same as the original one because of the threshold value at the analog out part. Generally, the upper and lower limit is ±16. Therefore, the output value needs to be properly reduced to fit the limit. In order to properly convey the analog signals to the digital controller, the gain part in Simulink can change the output value.

For the digital control, the feedback loop can be applied in dSPACE 1007 as a digital controller. Unlike the real-time simulator, dSPACE 1007 only processes digital signals in the whole system. That is to say, digital controller cannot directly identify the analog

signals generated by OPAL-RT 4500. Thus, the analog signals should be imported in the A/D board to realize the function as changing the analog signals into digital signals. In the tested platform, DS2003 A/D board is used as transferring the different kinds of signals. Besides, the dSPACE system will be automatically amplified the input value to 100 times. Therefore, it is suitable to set the reducing coefficient in OPAL-RT as 1 divided by 100.

Unlike dSAPCE, OPAL-RT can process both analog signals and digital signals. Therefore, there is no need to introduce any D/A board to the whole platform. This system will be implemented in the Hardware-In-the-loop(HIL).

In terms of scheduling, HIL simulation is less expensive and more practical than validation because you can set it up to run on its own. Fig.3-26 shows the whole HIL experimental simulation.

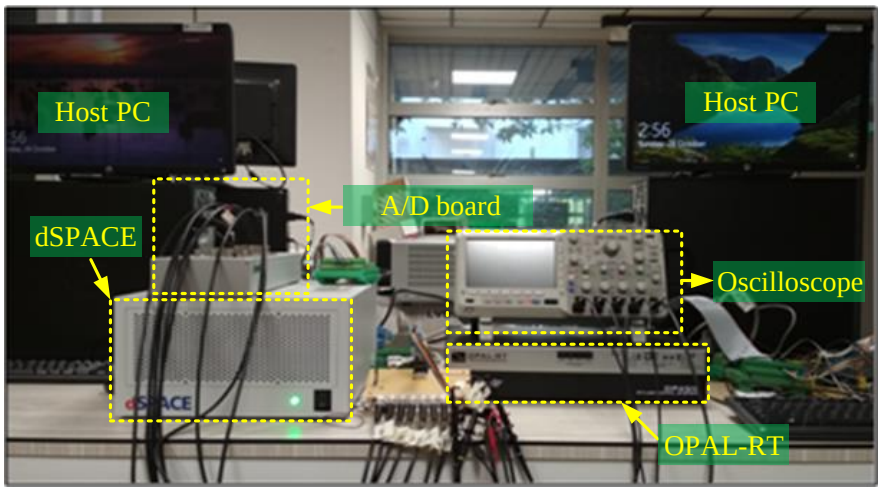

Fig. 3-26 HIL platform

As shown in the Fig.3-26, OPAL-RT platform is used to execute the whole plant in an analog control system. Then, the analog signals are transported into A/D board as the input signals of the dSPACE1007 platform. In the dSPACE platform, the controller is running in the digital control system. Finally, the oscilloscope was adopted to capture the

waveforms of grid current and voltage at PCC.

3.6 Summary

This chapter has introduced the series-connected adaptive stabilizer (SAS) under weak grid conditions and verified its superior capability to improve the stability of the system. At first, due to the varying grid condition, the instability issues cannot be perfectly addressed. Conversely, the introduction of an active power filter will deteriorate the system stability.

To deal with the instability issues, the SAS model is proposed subsequently. Both the function of the SAS model in the ideal case and the tested system are discussed. Eventually, experimental verifications are provided, which are consistent with the theoretical analysis.

Chapter 4 Hybrid Controlled LCL-type Grid-Connected Inverter

This chapter focuses on the hybrid controlling method(half digital and half analog) of grid-connected inverter, which has the same function as the active damping method. To begin with, the feedforward control method is reviewed. When considering the digital delay in the real world, the stability of GCI with a weak grid will also be affected. Then, the proposed hybrid controller, which consists of the analog control part and digital control part, is introduced to the grid-connected inverter. Through the Bode plot and Nyquist plot, it is suggested that the proposed hybrid controller is able to stabilize the inverter with a weak grid. At last, experimental verifications are provided, which are consistent with the theoretical analysis.

4.1 Revisiting Feedforward Control

According to the equation (3-5), the harmonics of grid voltage can lead to grid current harmonics. Therefore, feedforward current control, regarded as a virtual impedance in the active damping method, has been proposed to suppress the effect of voltage harmonics. In Fig.4-1, the block diagram of the inverter side with the feedforward loop is depicted.

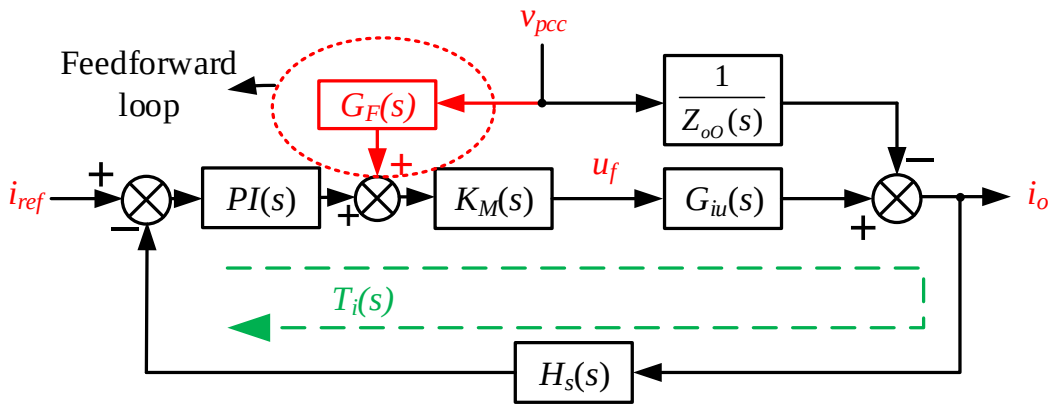

Fig. 4-1. Block diagram of inverter with feedforward loop

The block circled by the red line denotes the feedforward loop. As seen, it is a voltage controlled feedforward loop. The rest of the block diagram consists of the inverter model and a simple current controlled feedback loop. Therefore, the equivalent circuit of inverter with feedforward control is depicted as Fig.4-2.

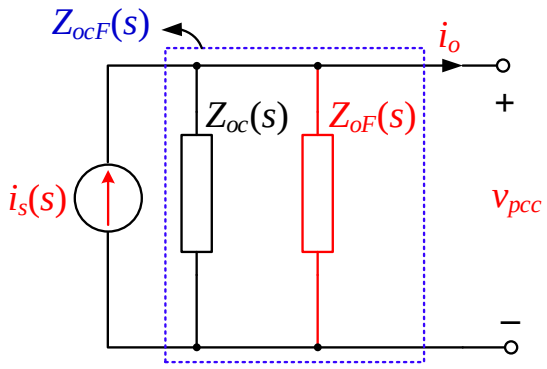

Fig. 4-2. Equivalent circuit of the inverter with feedforward control

As discussed in the literature review, the active damping method can generate a damper to suppress high-order harmonics without power loss. According to Fig.4-2, Z_{oF} denotes the virtual impedance generated by the feedforward loop. In order to effectively fix the harmonic issue, combined with equation (3-5), Z_{oF} should compensate to Z_{oC} to eliminate the part including voltage harmonics in (3-5). That improves the tuning of the feedforward coefficient called G_F.

After introducing feedforward control, the equivalent impedance of output impedance, in this case, Z_{oCF} should be designed to be infinite because of the previous discussion. The expressions of Z_{oCF} and Z_{oF} are shown as (4-1) and (4-2):

$$Z_{oCF}(s) = \frac{Z_{oC}(s) \cdot Z_{oF}(s)}{Z_{oC}(s) + Z_{oF}(s)} \tag{4-1}$$

$$Z_{oF}(s) = -\frac{\hat{v}_{pcc}}{\hat{i}_o}\bigg|_{\hat{u}_f=0} = -\frac{1}{G_F(s) \cdot K_M(s) \cdot G_{iu}(s)} \cdot \left[1 + T_i(s)\right] \tag{4-2}$$

From these two equations, the introduction of feedforward control can be regarded as a virtual impedance parallel connecting with inverter side impedance. According to the

previous discussion, if the overall impedance at the inverter side can be designed to be infinite, the equivalent circuit of the inverter can be regarded as an ideal current source. Therefore, in order to meet the requirement, the virtual impedance is referred to as (4-2) should satisfy the equation below:

$$Z_{oF}(s) = -Z_{oC}(s) \tag{4-3}$$

If the overall impedance should be infinite, combining with equation (4-1), the denominator should be set to zero, or the numerator should be set to infinite. The later one is not practical to be implemented. Thus, the equation (4-3) can be derived if the denominator is set to 0.

Similarly, according to (4-2), the feedforward coefficient can be derived as (4-4) combining with (3-15) and (3-16) easily:

$$G_F(s) = \frac{1}{K_M(s) \cdot Z_{oO}(s) \cdot G_{iu}(s)} \tag{4-4}$$

4.2 Effect of Digital Delay

In the digital control system, there are computation delay and pulse width modulation (PWM) delay[58]. The computation delay is the time duration from the sampling instant to the PWM reference update instant, and it is one sampling period in the synchronous sampling case (where the sampling takes place at the beginning and in the middle of a switching period). The computation delay is always one sampling period in the commonly used synchronous sampling scheme and is described as e^{-sT_S} [41]:

$$G_s(s) = e^{-sT_S} \tag{4-5}$$

PWM delay is caused by the zero-order hold (ZOH) effect which keeps the PWM reference constant after it has been updated, and it is approximately half sampling period

is described as $e^{-0.5sTs}$ [41].

$$G_{PWM}(s) = \frac{1 - e^{-sT_s}}{s \cdot T_s} \tag{4-6}$$

The derivation of (4-6) needs to be clearly demonstrated. The exponential function with base *e* has Maclaurin series as (4-7):

$$e^x = \sum_{n=0}^{\infty} \frac{x^n}{n!} = 1 + x + \frac{x^2}{2!} + \frac{x^3}{3!} + \cdots + \frac{x^n}{n!} \tag{4-7}$$

Besides, when the value of *x* (which is the variable in the equation) tends to zero, the exponential function can be approximately simplified as:

$$\lim_{x \to 0} e^x = 1 + x \tag{4-8}$$

The time step in the tested system is small enough so that most of the equation parts can be ignored to get the approximation. Therefore, the numerator of equation (4-6) can be rewritten as (4-9):

$$\begin{aligned} &\lim_{x \to 0}\left(1 - e^{-sT_s}\right) = \lim_{x \to 0}\left(1 - e^{0.5sT_s} \cdot e^{-0.5sT_s}\right) = \lim_{x \to 0}\left(1 - \frac{e^{-0.5sT_s}}{e^{0.5sT_s}}\right) \\ &= 1 - \frac{1 + \left(-0.5sT_s\right)}{1 + 0.5sT_s} = \frac{sT_s}{1 + 0.5sT_s} \end{aligned} \tag{4-9}$$

Subsisting (4-9) into the expression of PWM delay, the approximation can be derived. Accordingly, the equation (4-6) can be reformulated as (4-10):

$$\begin{aligned} G_{PWM}(s) &= \frac{1 - e^{-sT_s}}{s \cdot T_s} \\ &\approx \frac{\frac{sT_s}{1 + 0.5sT_s}}{s \cdot T_s} = \frac{1}{1 + 0.5sT_s} = \frac{1}{e^{0.5sT_s}} = e^{-0.5sT_s} \end{aligned} \tag{4-10}$$

The whole system is implemented in the digital control system, so the problem of digital delay must be considered in the control loop. When considering digital delay, the whole block diagram with digital delay, which is shown in Fig.4-3, contains these two kinds of delay, and the digital delay changes the transfer function of both feedback and feedforward loop.

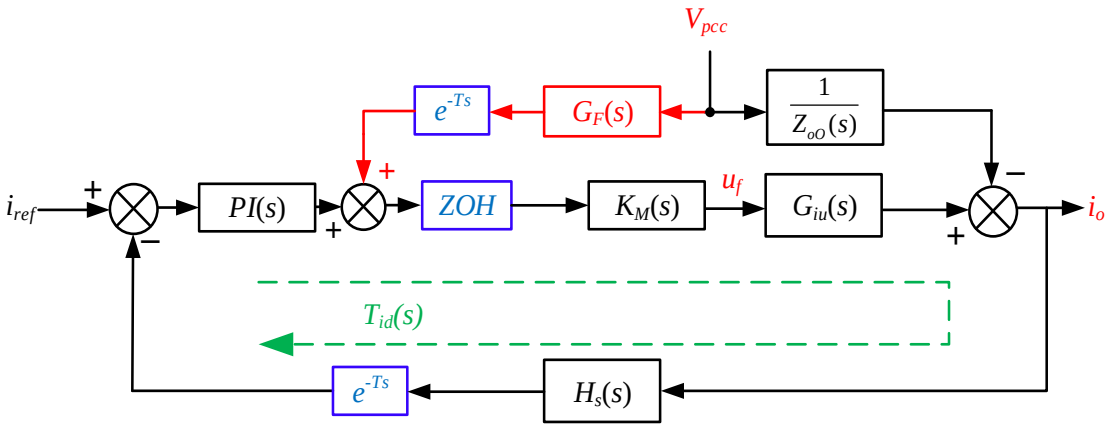

Fig. 4-3. Block diagram of inverter considering the digital delay

According to Fig.4-3, the digital delay is considered in feedback and feedforward control loop. Blue blocks refer to two kinds of a digital delay. The PWM delay has been considered in the process of gate signal generation. $T_{id}(s)$ denotes the loop gain of closed-loop with digital delay:

$$T_{id}(s) = T_i(s) \cdot G_s(s) \cdot G_{ZOH}(s) = T_i(s) \cdot e^{-1.5sT_s} \tag{4-11}$$

It is indicated that the loop gain is delayed by one and a half time step according to (4-11). Similarly, the feedforward loop will also be delayed for one and a half time steps, as shown in Fig.4-3.

Since the loop gain is affected because of digital delay, the impedance of the inverter side will certainly be affected. According to the block diagram, the equivalent circuit of the inverter can be derived as Fig.4-4:

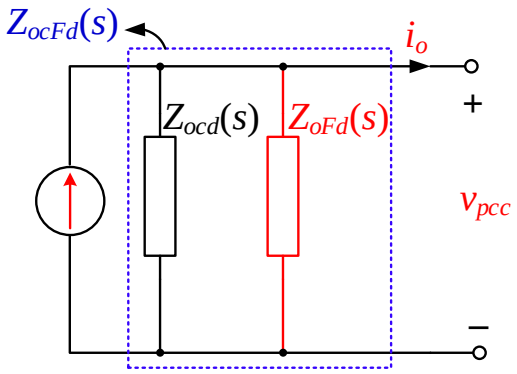

Fig. 4-4. Equivalent circuit of inverter considering the digital delay

Z_{oCd} denotes the closed-loop output impedance of the inverter with digital delay, which is shown as (4-12). Z_{oFd} refers to the feedforward loop output impedance with digital delay, which is shown as (4-13). Z_{oCFd} is equal to the final output impedance with digital delay, which is shown as (4-14):

$$Z_{oCd}(s) = Z_{oO}(s) \cdot \left[1 + T_{id}(s)\right] \tag{4-12}$$

$$Z_{oFd}(s) = -\frac{1}{e^{-1.5sT_S} \cdot G_F(s) \cdot K_M(s) \cdot G_{iu}(s)} \cdot \left[1 + T_{id}(s)\right] = -Z_{oCd}(s) \cdot e^{1.5sT_S} \tag{4-13}$$

$$Z_{oCFd}(s) = \frac{Z_{oCd}(s) \cdot Z_{Fd}(s)}{Z_{oCd}(s) + Z_{Fd}(s)} = \frac{Z_{oCd}(s) \cdot \left[-Z_{oCd}(s) \cdot e^{1.5sT_s}\right]}{Z_{oCd}(s) - Z_{oCd}(s) \cdot e^{1.5sT_s}} = \frac{1}{1 - e^{-1.5sT_s}} \cdot Z_{oCd}(s) \tag{4-14}$$

Z_{Fd} refers to the virtual impedance with consideration of digital delay. These two kinds of delay not only change the characteristic of the resonance damping but also degrade the control performance of the designed feedforward loop.

Due to the digital delay, the loop gain, output impedance of the inverter and virtual impedance of the feedforward loop are shaped. Moreover, according to (4-14), the designed feedforward coefficient cannot compensate for the output impedance to obtain an ideal current source. To clarify the effect of the digital delay, the Bode plot of the transfer function caused by digital delay is presented as Fig.4-5:

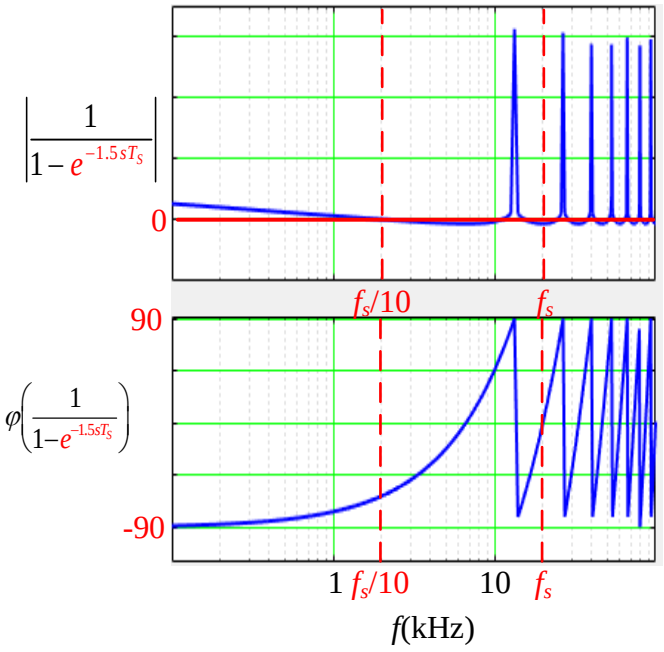

Fig. 4-5. Bode plot of Z_{delay}

As shown in Fig.4-5, the magnitude of Z_{delay} is positive below $f_s/10$, which means it can only promise and improve the performance of the control loop at the low-frequency range. However, the different part caused by digital delay introduces almost 90 degrees phase lag to the original system below $f_s/10$.

Moreover, the phase of delay part is oscillating between positive 90 degrees and negative 90 degrees at around sampling frequency f_s, which is equal to 20kHz.

$$Z_{delay} = \frac{1}{1-e^{-1.5sT_s}} \tag{4-15}$$

The Bode plot of inverter side impedance, grid side impedance with and without digital delay are illustrated in Fig.4-6(a). After introducing the digital delay in the feedforward loop, the phase response is effected and decreased by 90 degrees at around the crossover frequency. The phase lag caused by the digital controlled feedforward loop indeed influences the phase margin of the system, which leads to instability issues to the inverter.

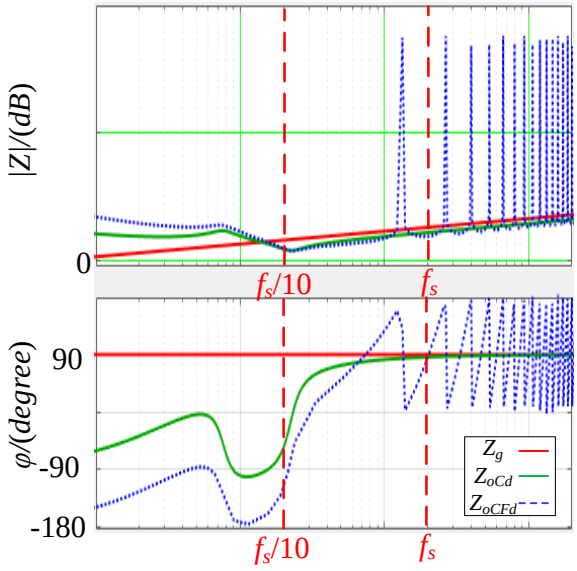

(a)

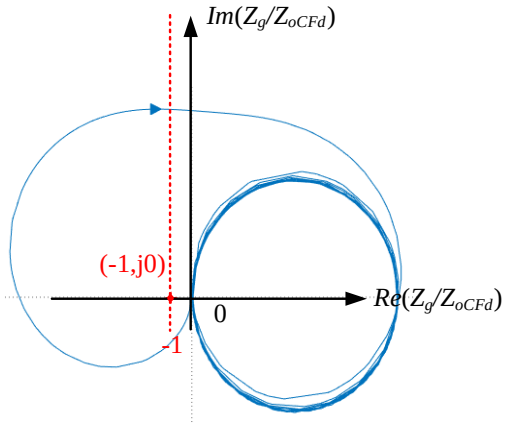

(b)

Fig. 4-6. Digital feedforward: (a)Bode plot; (b)Nyquist plot

Moreover, the frequency response of Z_{delay} also reflects the attenuated capability of the digital controlled feedforward loop to suppress the harmonics. As seen, the magnitude of is amplified, especially when the frequency is higher than 10kHz.

In Fig.4-6(b), the Nyquist plot shows that the GCI with a weak grid considering digital delay is not stable because it encircles (-1, j0). However, there is no timing sampling in the analog control system and the signal change is real-time and continuous, the problem

of delay does not exist in the analog control. Thus, the application of hybrid digital-analog control is practical to ensure the stability of the grid-connected inverter, which is proposed in the following sections.

Therefore, Fig.4-6 shows the performance testing when introducing the digital delay in the GCI with weak grid conditions. Thus, eliminating the effect of digital delay is one of the most challenging goals in the design of the controller.

4.3 Hybrid Control Method

Based on the above discussion, the digital controlled feedforward method will lead to instability issues if applied. Therefore, the whole control loop cannot be implemented in the digital controller. That is the reason for applying the hybrid control method.

For the analog control system, it mainly deals with continuous signals that can take a wide range of values. The transfer function is given by the differential equation in the s-domain. Moreover, the noise, interference and distortion is comparatively more. Therefore, power efficiency or quality is comparatively less (because of continuous signals). Because the storage, analysis, and processing of data are complicated comparing with digital control, most of the control method is applied in the digital control system[61].

For the digital control system, it deals with binary or discrete signals having values 1 or 0. Their input-output relationship (transfer function) are represented by a different equation in the z-domain. Noise, interference, and distortion are comparatively less in the case of digital control systems[43]. Power efficiency is more than it is in the analog control system. Storage, analysis, and processing of data are easy and convenient which is a superior advantage comparing with analog control[23]. Therefore, it is widely used as it is easy to handle and operate.

However, when applied in the digital control system, there are some problems such as digital delay, as previously mentioned. In order to address the instability problems caused by digital delay and weak grid conditions, a hybrid controlled LCL-type GCI is presented in this report. Therefore, both digital control and analog control are used in this method to achieve better performance.

According to the discussion in the previous part, only digital control will bring many issues. Although it is hard to consider the effect of digital delay, the digital delay part can be simplified as a transfer function discussed in the previous chapter.

Moreover, it is an effective approach to achieve hybrid control because full-analog control is hard to implement in industry application, while full-analog control may have better performance. Thus, both the feedforward loop and feedback loop are used to generate four gate signals. Therefore, the input gate signals are the sum of signals generated by two control systems respectively. The whole loop is shown as Fig.4-7:

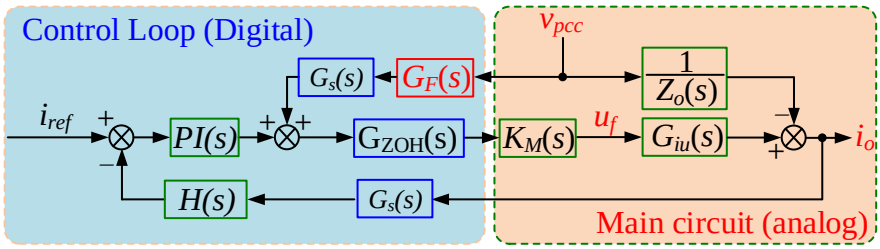

Fig. 4-7. Block diagram of the hybrid control method

The hybrid control method separates the whole control system into analog control and digital control system. According to the effect of digital delay, the hybrid control method is analyzed in the following procedure to ensure performance.

The hybrid control method is designed to separate the system into an analog controlled feedforward loop and digital controlled feedback loop. The block diagram and equivalent circuit of Hybrid control method are shown in Fig.4-8 and Fig.4-9:

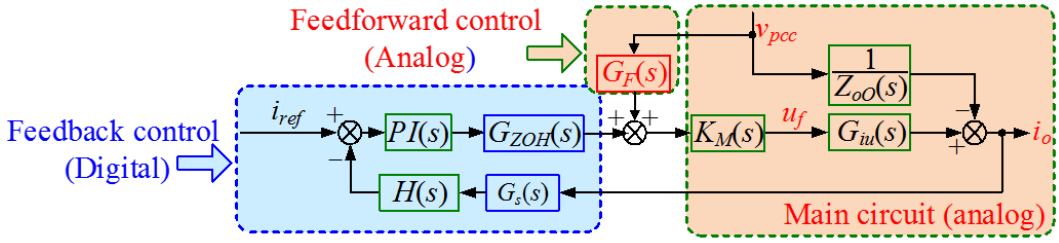

Fig. 4-8. Block diagram of Hybrid control method

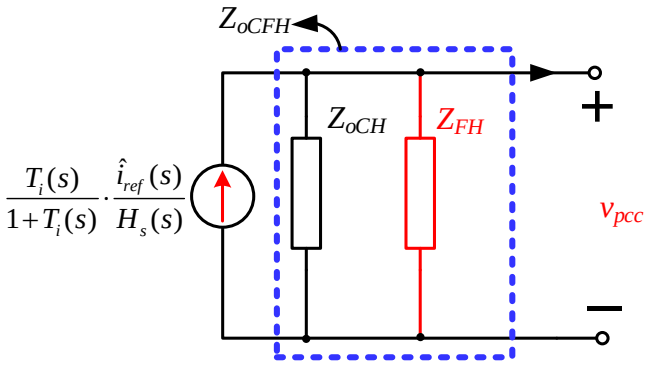

Fig. 4-9. Equivalent circuit of Hybrid control method

In Fig.4-9, $Z_{oCH}(s)$ refers to the original closed-loop output impedance of hybrid control method, $Z_{FH}(s)$ refers to the virtual impedance of feedforward loop with hybrid control method, $Z_{oCH}(s)$ can be expressed as (4-16):

$$Z_{oCH}(s) = Z_o(s) \cdot \left[1 + T_{id}(s)\right] \tag{4-16}$$

$$Z_{FH}(s) = -\frac{1+T_{id}(s)}{G_F(s) \cdot G_{iu}(s) \cdot K_M(s)} = -Z_{oO}(s) \cdot \left[1+T_{id}(s)\right] = -Z_{oCH}(s) \tag{4-17}$$

$$Z_{oCFH}(s) = \frac{Z_{oCH}(s) \cdot Z_{FH}(s)}{Z_{oCH}(s) + Z_{FH}(s)} \approx \infty \tag{4-18}$$

The hybrid control method can make the equivalent impedance of whole circuit $Z_{oCFH}(s)$ to infinite so that the effect of grid voltage harmonics can be suppressed. This function cannot be designed by only introducing the digital delay in the feedforward loop. Therefore, the hybrid control method is effective in dealing with the instability issue caused by a weak grid and digital delay.

Admittedly, the implementation of the analog part is more complicated than that of the digital part. For instance, if we want to obtain an ideal sinusoidal wave as a carrier wave, it is much easier to realize it in the digital system rather than in analog system. Therefore, in order to simplify the implementation, the transfer function of the feedforward coefficient can be divided into three parts as follows:

$$G_F(s) = \underbrace{\frac{V_{tri}}{V_{dc}}}_{G_{F1}} + \underbrace{\frac{sC_fR_1}{1+sC_fR_c}\cdot\frac{V_{tri}}{V_{dc}}}_{G_{F2}} + \underbrace{\frac{s^2C_fL_1}{1+sC_fR_c}\cdot\frac{V_{tri}}{V_{dc}}}_{G_{F3}} \tag{4-19}$$

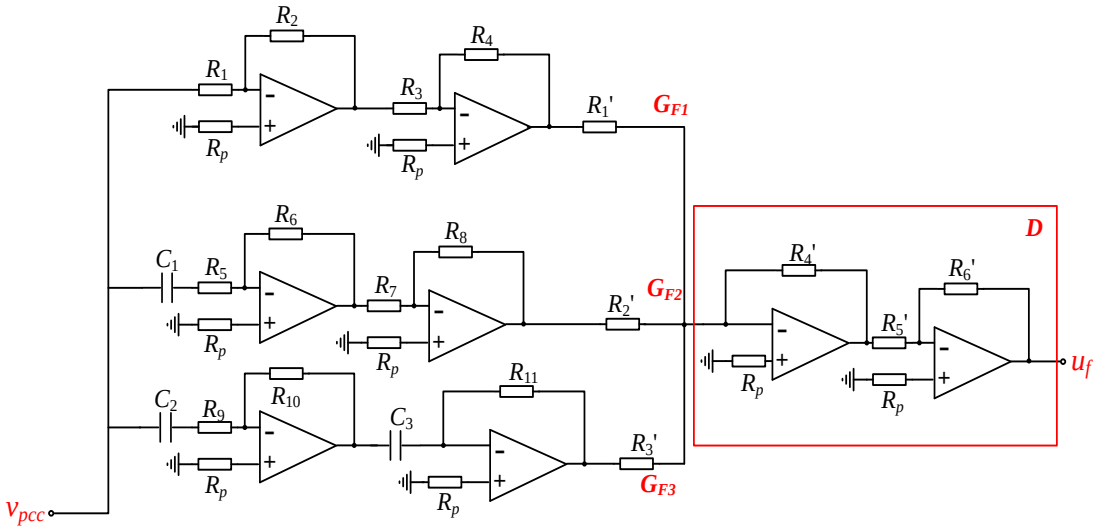

Fig. 4-10. Implementation of analog feedforward loop

Fig.4-10 presents the analog implementation of the feedforward loop using op-amps. G_{F1} can be realized using a non-inverting op-amp. G_{F2} can be realized using one differential op-amp and one inverting op-amp. G_{F3} can be realized using two differential op-amps. Block D refers to a block function as a summing block, which sums up two inverting op-amps.

4.4 Experimental Verifications

The stability of GCI with weak grid and hybrid control method will be experimentally

investigated in this section.

At first, the digital controlled feedforward method is applied to the whole system which is proved to illustrate the negative effect of introducing the digital delay. Thus, the hybrid control method is proposed as an effective approach to remove the effect. Furthermore, the effectiveness of the proposed modified hybrid control method for system stability enhancement will also be verified.

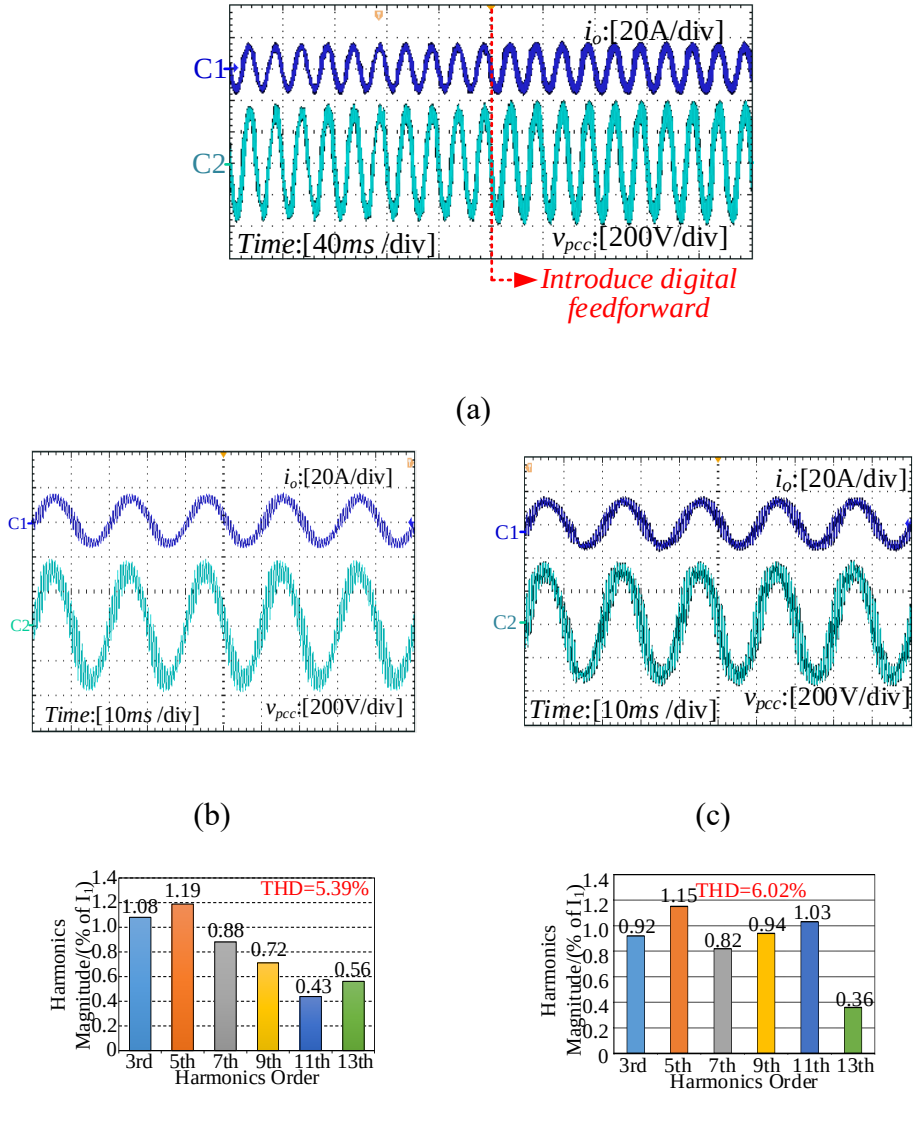

Fig. 4-11. The experimental result of introducing digital feedforward: a) Introducing hybrid control; b) System with only feedback control; c) System with digital feedforward; d) THD of current without digital feedforward; e) THD of current with digital feedforward control

Fig.4-11 shows the performance testing result of introduced digital controlled feedforward control. As shown in Fig. 4-11(b) and Fig. 4-11(c), the introduced digital feedforward control leads to severe distortion of grid current. In Fig. 4-11(d) and Fig. 4-11(e), the THD of the current can also prove that digital feedforward control will deteriorate the instability issues. Moreover, according to the bode plot and Nyquist plot shown in the previous discussion, the digital feedforward loop cannot address instability issues. Thus, it is not an improvement.

As for the hybrid control system, the overall control loop with the hybrid control method can suppress current harmonics and maintain stability, as discussed in the previous discussion. If the experiment results below show the same conclusion as the previous discussion, then the hybrid control system is proved as a practical way to solve these problems.

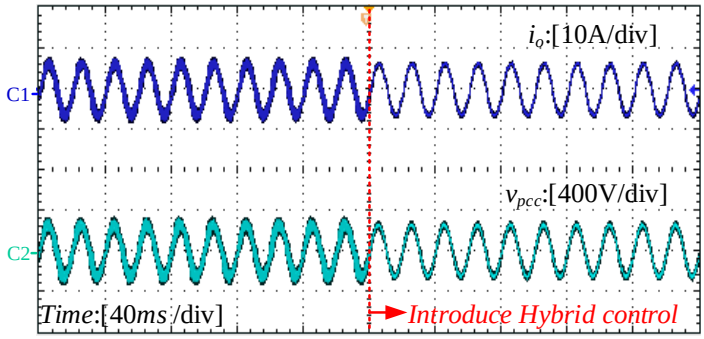

(a)

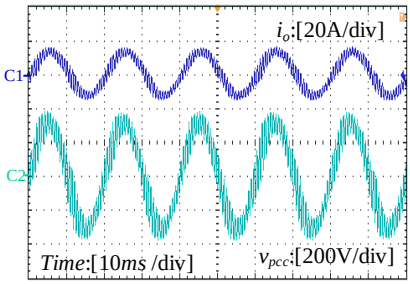

(b)

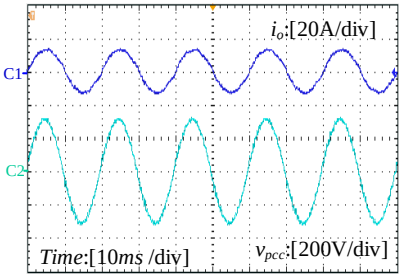

(c)

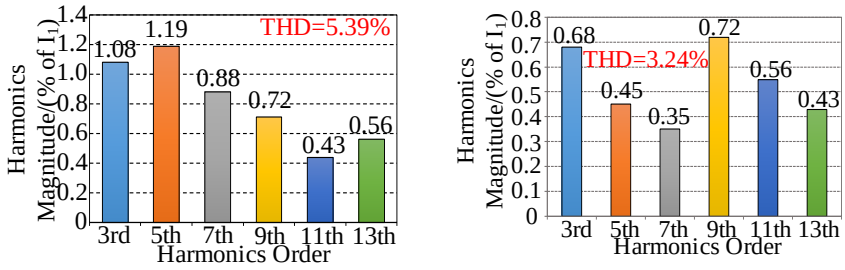

(d) (e)

Fig. 4-12. The experimental result of the hybrid control: a) Introducing hybrid control at 2.5s; b) System with only digital feedback control; c) System with hybrid control; d) THD of current with digital control; e) THD of current with hybrid control.

Fig.4-12 shows the performance testing results of the hybrid control method. Fig.4-12(a) shows a dynamic waveform of introducing hybrid control at 2.5s. As shown in Fig.4-12(a), the proposed hybrid control method is introduced at 2.5s. The waveform at the steady-state is shown as Fig.4-12(b) and Fig.4-12(c). When introducing hybrid control, both current and voltage waveform shows less ripple than before. The consequence is the same as the previous discussion. It proves that digital-feedforward will deteriorate the performance of GCI, while proposed hybrid control can be designed to attenuate harmonics and maintain stability. Besides, Fig.4-12(d) and Fig.4-12(e) shows the specific results of THD of current. Moreover, THD of current also verifies the correctness of proposed hybrid control.

4.5 Summary

This chapter firstly introduces the feedforward control as an active damping method in order to shape the inverter side impedance. The design procedures are specified based on the impedance-based stability criterion. Due to the effect of digital delay, the inverter side impedance cannot be infinite and therefore cause instability issues combining with weak grid conditions.

Therefore, the hybrid control method is proposed to address the issues above. Besides, the specific analog implementation of the feedforward loop is presented. The simulation results prove that the negative effect of digital delay and the correctness of the proposed

hybrid control scheme.

Chapter 5 Conclusion and Future Research

This chapter summarizes the conclusions of this thesis. It provides recommendations for future research in terms of the application of series-connected stabilizer in three-phase inverter, parallel inverters system and even microgrid. The conclusions of this thesis are listed below:

(1) In the condition of a weak grid, the harmonic and instability issues are severe for the system and performance of the inverter.
(2) For the grid side, a series-connected SAS model has been presented. It is proved that the SAS method is feasible to address the instability problem comparing with traditional APF and is adaptive to weak grid conditions.
(3) For the inverter side, a hybrid controlled LCL type grid-connected inverter is proposed to deal with instability issues caused by the weak grid and digital delay as an active damping method.

Based on the practical application of proposed series-connected adaptive stabilizer, the future research discussion is presented in this chapter as follows:

(1) Application in three-phase inverter with weak grid
(2) The design procedure of SAS in parallel inverters system
(3) The effect of the SAS model in microgrid

5.1 Conclusions

In this thesis, the impedance shaping methods, which are proposed as a practical approach to address harmonic and instability issues, are presented in the weak grid condition. The impedance shaping method can be summarized as shaping grid side impedance and shaping inverter side impedance, respectively. Subsequently, the conclusion can be obtained as follows.

Firstly, the series active power filter cannot perfectly deal with the instability issues in the weak grid condition but deteriorate the performance of the inverter. Moreover, in the real world, the parameters of the control loop and filters are different. Therefore, for the grid side, a series-connected SAS model has been presented. The whole model acts as an equivalent impedance to solve the instability problem caused by impedance mismatching in a weak grid. Unlike traditional SAPF, proposed SAS aims at maintaining stability. SAS model only contains an adaptive current-controlled loop, including a frequency regulation circuit that is easily applied. It is pointed out that the proposed scheme is designed to adaptively adopt two different control loops, which are mainly deal with harmonics issues and instability issues, respectively. Finally, according to implementation in both stable and unstable conditions, it is proved that the SAS method is feasible to address the instability problem.

For the inverter side, unlike the grid side, a hybrid controlled LCL type grid-connected inverter is proposed in order to suppress the harmonics and maintain the stability of the system under weak grid conditions. In the beginning, the principle of feedforward control is reviewed as a successful active damping method. However, the introduction of digital delay may further affect the stability of the inverter and therefore leads to instability issues. According to the discussion of the hybrid control method, it is shown that the hybrid control can effectively eliminate the effect of digital delay and therefore improve the performance of the inverter. Moreover, the simulation proves the correctness of discussion.

5.2 Future Research

5.2.1 Application in Three-phase grid-connected inverter

The basic idea of the control strategy of the conventional three-phase active power filter is: set three-phase current references for the three-phase input phase current, which are

in phase with the phase voltage, include only the fundamental wave, and have the same amplitude as each other. By controlling each phase converter, the phase currents i_a, i_b, i_c follow the reference and change within a different band. Because the reference is a sine wave with the same amplitude and the same phase as the phase voltage, the phase currents i_A, i_B, and i_C are currents with high power factor, small distortion, and symmetric current when the switching frequency band is filtered by the additional passive filter, such as LC filter.

If the loss of the active filter is ignored, in a steady-state, the energy consumed by the load is equal to the energy generated by the power supply. That is to say, the input and output power remain balanced. The capacitor on the DC-link is an energy storage element, so the grid-connected inverter can exchange energy with the power grid and the load. The reactive power required by the load is obtained through the exchange with the active power filter. Reactive power is only exchanged between the active power filter and the load. The asymmetric power required by the load is provided to the load by the power supply after energy exchange between the phases of the converter.

If the input and output power are out of balance, the energy in the unbalanced part will be recharged or absorbed by the DC-link capacitor, which will lead to the capacitor voltage distortion. If the active power supplied by the power supply is less than the load needs, the DC capacitor voltage will drop, and the control circuit will increase the amplitude of the current reference of each phase at the same time after detecting the decline in the capacitor voltage to increase the active power supply.

Conversely, when the DC-link capacitor voltage rises, the amplitude of the current reference of each phase will be reduced at the same time. Finally, the supply and demand for energy will reach a balance. The average value of the capacitor voltage on the DC bus provides information on whether the power is balanced. The feedback control is widely used to determine the amplitude of the reference value of the current to achieve a

balance between input and output power.

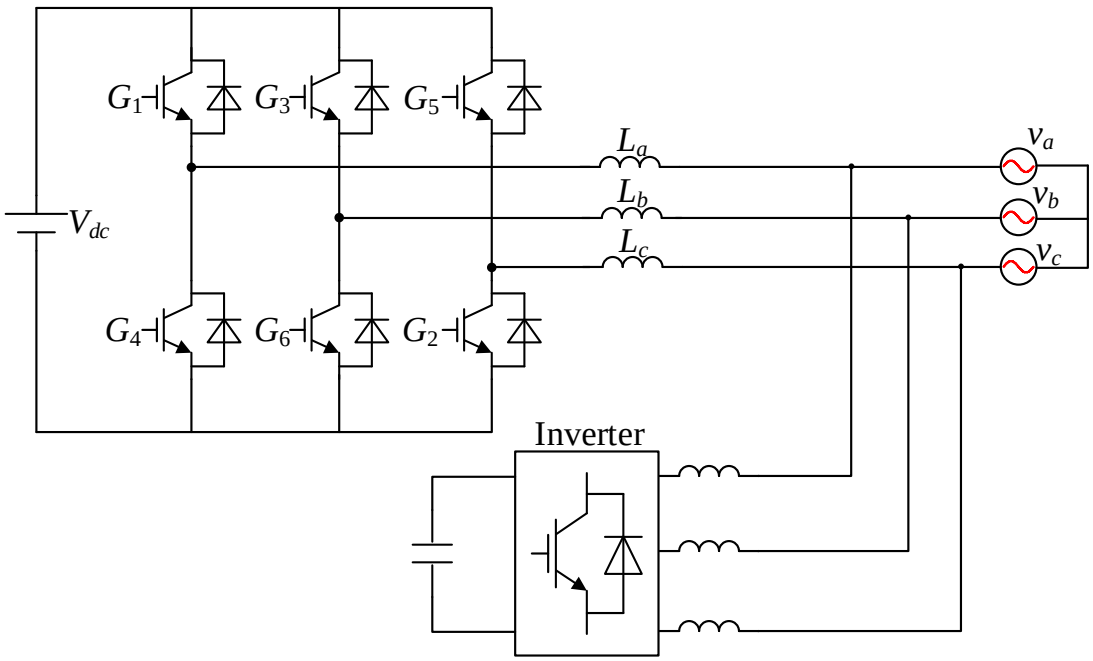

Fig. 5-1. Three-phase inverter with shunt active power filter

Fig. 5-1 demonstrates the basic topology of a three-phase inverter with shunt active power filter. However, there are several novel control scheme applied in the control of APF. In [70], a shunt active power filter is applied in the three-phase rectifier in order to compensate for the current harmonics caused by the non-linear loads at the grid side. To improve the performance of shunt APF, an adaptive neural network (ADNN) is used to detect the THD of current.

[71] proposes a topology of a single-phase inverter to act as a three-phase active power filter. It directly connects the third leg of the three-phase active power filter with the negative side of the capacitor.

Moreover, [72] proposes a novel control scheme to predict the current. The additional control scheme can compensate the error due to the parameter variation. Besides, it is proved that the performances in steady-state and load variation are great.

Unlike shunt active power filters, series-connected active power filters show less power loss and should be applied in three-phase system. The control method of the proposed active power filter should be tested in the future work. If the proposed SAS model is implemented as three individual active power filter, the control method could be the same as the control scheme mentioned before. If the topology of the active power filter is different, such as three-phase four-wire active power filter, the control loop needs to be redesigned. Therefore, in the future work, the proposed SAS model will be improved, and the topology of it will be the same as series-connected active power filter to achieve high efficiency.

5.2.2 Parallel Inverters System

It will be important that future research investigates the feasibility of the SAS model application. For instance, application in a three-phase inverter system. When it comes to the three-phase inverters system, the position, locking logic, and parameters may not be the same as the condition of single-phase. Therefore, it is a new research topic of future research to investigate it.

Moreover, the parallel-inverter system needs to be considered in future research. The paralleled inverters may be unstable due to the interaction among these inverters or cables [73]. In [73], a generic stability impedance criterion has been proposed without any assumptions. Therefore, it can evaluate the stability of any types of parallel inverters with different inverter parameters and both long and short cables. It is a practical criterion to utilize the criterion for control design.

How to effectively reduce the circulating current and to accurately share power among parallel inverters became a critical problem to be addressed [74]. In this paper, an inverter (RC type inverter) using a resistor-capacitor output impedance is proposed, which not only provides fast reactive power-sharing to support the microgrid voltage, but also

reduces the circulating current and the damping high-frequency resonance of inverters due to different equivalent output impedance of inverter, and line impedances.

Moreover, droop control is a well-known strategy for parallel operation of inverters [75]. In [75],the proposed control method can derive a small-signal model of parallel inverters model whose impedance angle is between $-\pi/2$ rad and $\pi/2$ rad. Thus, it can be applied to any practical inverters having an impedance angle between $-\pi/2$ rad and $\pi/2$ rad.

[76] proposes an orthogonal impedance-sharing control, which can dynamically adjust the phase and magnitude of the effective impedance. Through the control method, harmonic currents of nonlinear loads are designed to be properly shared among parallel inverters by shaping the effective harmonic impedance. Moreover, unlike droop control, it can be widely used in different impedance conditions (such as different line impedance).

As for multi-inverter condition, the application of the SAS model needs to be improved because of series impedance, parallel impedance, and grid impedance. Besides, the attenuation of circulating current and harmonic current sharing performance is critical to be considered in the design of GCI. Another improvement could be the dynamic performance of the SAS model. Since the waveform of the grid-connected inverter with SAS model shows oscillations after introducing SAS model, the parameters of the PI controller in the adaptive frequency regulation circuit should be tuned carefully again to ensure the dynamic performance.

Author's Publication

B. Zhao, X. Zhang and L. Miao, "Adaptive Impedance Shaping Method for Improving LCL-type GCI under Weak Grid," 2019 IEEE 4th International Future Energy Electronics Conference (IFEEC), Singapore, Singapore, 2019, pp. 1-5.

L. Miao, J. Z. Xin and **B. Zhao**, "Revisit Nyquist-Bode Stability Criteria for Power Electronic System with Non-minimum Phase System," 2019 IEEE 4th International Future Energy Electronics Conference (IFEEC), Singapore, Singapore, 2019, pp. 1-6.

F. Feng, X. Zhang, P. Gao, F. Lin, **B. Zhao** and H. B. Gooi, "Impedance Modeling and Stability Analysis of Triple-Phase-Shift-Based Dual Active Bridge Converter with LC Filter," 2019 10th International Conference on Power Electronics and ECCE Asia (ICPE 2019 - ECCE Asia), Busan, Korea (South), 2019, pp. 1128-1132.

Bibliography

[1] V. Telukunta, J. Pradhan, A. Agrawal, M. Singh and S. G. Srivani, "Protection challenges under bulk penetration of renewable energy resources in power systems: A review," in *CSEE Journal of Power and Energy Systems*, vol. 3, no. 4, pp. 365-379, Dec. 2017.

[2] F. Blaabjerg, R. Teodorescu, M. Liserre, and A. V. Timbus, "Overview of Control and Grid Synchronization for Distributed Power Generation Systems," *IEEE Transactions on Industrial Electronics*, vol. 53, no. 5, pp. 1398-1409, 2006.

[3] Hannah Ritchie and Max Roser (2020) - "Renewable Energy". Published online at OurWorldInData.org.

[4] H. Yin, X. Guanghan, H. Xuan and H. Wangyun, "Research on Harmonic Suppression Strategy of Grid - Connected Inverter Based on Power Grid Background Harmonics," *2018 International Conference on Engineering Simulation and Intelligent Control (ESAIC)*, Changsha, 2018, pp. 286-289.

[5] X. Chen, X. Ruan, D. Yang, W. Zhao and L. Jia, "Injected Grid Current Quality Improvement for a Voltage-Controlled Grid-Connected Inverter," in *IEEE Transactions on Power Electronics*, vol. 33, no. 2, pp. 1247-1258, Feb. 2018.

[6] Jana, J., Saha, H., & Bhattacharya, K. D. (2017). A review of inverter topologies for single-phase grid-connected photovoltaic systems. *Renewable and Sustainable Energy Reviews*, *72*, 1256-1270.

[7] Z. Ni, Q. Qian, S. Xie, J. Xu and B. Zeng, "Harmonic Suppression and Stability Enhancement for Grid-Connected Inverters Based on UPQC," *2018 IEEE Energy Conversion Congress and Exposition (ECCE)*, Portland, OR, 2018, pp. 4922-4926.

[8] D. Yang, X. Ruan and H. Wu, "Impedance Shaping of the Grid-Connected Inverter with LCL Filter to Improve Its Adaptability to the Weak Grid Condition," in *IEEE Transactions on Power Electronics*, vol. 29, no. 11, pp. 5795-5805, Nov. 2014.

[9] Büyük, M., Tan, A., Tümay, M., & Bayındır, K. Ç. (2016). Topologies, generalized designs, passive and active damping methods of switching ripple filters for voltage source inverter: A comprehensive review. *Renewable and Sustainable Energy Reviews*, *62*, 46-69.

[10] R. Peña-Alzola, M. Liserre, F. Blaabjerg, R. Sebastiá́n, J. Dannehl and F. W. Fuchs, "Analysis of the Passive Damping Losses in LCL-Filter-Based Grid Converters," in *IEEE Transactions on Power Electronics*, vol. 28, no. 6, pp. 2642-2646, June 2013.

[11] C. Zou, B. Liu, S. Duan and R. Li, "Influence of Delay on System Stability and Delay Optimization of Grid-Connected Inverters With LCL Filter," in *IEEE Transactions on Industrial Informatics*, vol. 10, no. 3, pp. 1775-1784, Aug. 2014.

[12] S. B. Kjaer, J. K. Pedersen and F. Blaabjerg, "A review of single-phase grid-connected inverters for photovoltaic modules," in *IEEE Transactions on Industry Applications*, vol. 41, no. 5, pp. 1292-1306, Sept.-Oct. 2005.

[13] W. Choi et al., "Reviews on grid-connected inverter, utility-scaled battery energy storage system, and vehicle-to-grid application - challenges and opportunities," *2017 IEEE Transportation Electrification Conference and Expo (ITEC)*, Chicago, IL, 2017, pp. 203-210.

[14] Y. Han *et al*., "Modeling and Stability Analysis of LCL -Type Grid-Connected Inverters: A Comprehensive Overview," in *IEEE Access*, vol. 7, pp. 114975-115001, 2019.

[15] X. Liang and C. Andalib -Bin- Karim, "Harmonics and Mitigation Techniques Through Advanced Control in Grid-Connected Renewable Energy Sources: A Review," in *IEEE Transactions on Industry Applications*, vol. 54, no. 4, pp. 3100-3111, July-Aug. 2018.

[16] U. P. Yagnik and M. D. Solanki, "Comparison of L, LC & LCL filter for grid connected converter," *2017 International Conference on Trends in Electronics and Informatics (ICEI)*, Tirunelveli, 2017, pp. 455-458.

[17] R. N. Beres, X. Wang, M. Liserre, F. Blaabjerg and C. L. Bak, "A Review of Passive Power Filters for Three-Phase Grid-Connected Voltage-Source Converters," in *IEEE Journal of Emerging and Selected Topics in Power Electronics*, vol. 4, no. 1, pp. 54-69, March 2016.

[18] H. M. Kojabadi, B. Yu, I. A. Gadoura, L. Chang and M. Ghribi, "A novel DSP-based current-controlled PWM strategy for single phase grid connected inverters," in *IEEE Transactions on Power Electronics*, vol. 21, no. 4, pp. 985-993, July 2006.

[19] E. Şehirli and M. Altinay, "Input — Output linearization control of three — Phase

voltage source PWM rectifier using L and LCL filter," *45th International Universities Power Engineering Conference UPEC2010*, Cardiff, Wales, 2010, pp. 1-6.

[20] W. Yao, Z. Lu, H. Long and B. Li, "Research on grid-connected interleaved inverter with L filter," *2013 1st International Future Energy Electronics Conference (IFEEC)*, Tainan, 2013, pp. 87-92.

[21] R. Xie, X. Hao, X. Yang, L. Huang, C. Wang and Y. Yang, "Stability analysis of single-phase grid-connected inverter with L-filter," *2014 IEEE Energy Conversion Congress and Exposition (ECCE)*, Pittsburgh, PA, 2014, pp. 5626-5630.

[22] Q. Zhang, Y. Tang, L. Hou, F. Deng, S. An and X. Sun, "An Active High Frequency Damping Scheme for the Current Control of L Filter-Based Grid-Connected Inverter," in *IEEE Access*, vol. 7, pp. 171738-171751, 2019.

[23] T. Kawabata, T. Miyashita and Y. Yamamoto, "Digital control of three-phase PWM inverter with LC filter," in *IEEE Transactions on Power Electronics*, vol. 6, no. 1, pp. 62-72, Jan. 1991.

[24] T. G. Habetler, R. Naik and T. A. Nondahl, "Design and implementation of an inverter output LC filter used for dv/dt reduction," in I*EEE Transactions on Power Electronics*, vol. 17, no. 3, pp. 327-331, May 2002.

[25] G. Lo Calzo, A. Lidozzi, L. Solero and F. Crescimbini, "LC filter design for on-grid and off-grid distributed generating units," in *IEEE Transactions on Industry Applications*, vol. 51, no. 2, pp. 1639-1650, March-April 2015.

[26] T. Kuczek, M. Florkowski and W. Piasecki, "Transformer Switching With Vacuum Circuit Breaker: Case Study of PV Inverter LC Filters Impact on Transient Overvoltages," in *IEEE Transactions on Power Delivery*, vol. 31, no. 1, pp. 44-49, Feb. 2016.

[27] S. Jayalath and M. Hanif, "An LCL-Filter Design With Optimum Total Inductance and Capacitance," in *IEEE Transactions on Power Electronics*, vol. 33, no. 8, pp. 6687-6698, Aug. 2018.

[28] Y. Kim and H. Kim, "Optimal design of LCL filter in grid-connected inverters," in *IET Power Electronics*, vol. 12, no. 7, pp. 1774-1782, 19 6 2019.

[29] Y. Jiao and F. C. Lee, "LCL Filter Design and Inductor Current Ripple Analysis

for a Three-Level NPC Grid Interface Converter," in *IEEE Transactions on Power Electronics*, vol. 30, no. 9, pp. 4659-4668, Sept. 2015.

[30] S. Jayalath and M. Hanif, "Generalized LCL-Filter Design Algorithm for Grid-Connected Voltage-Source Inverter," in *IEEE Transactions on Industrial Electronics*, vol. 64, no. 3, pp. 1905-1915, March 2017.

[31] C. Zheng et al., "Integrated design method for LCL-type filter and current controller to improve inverter adaptability to grid impedance," in *IET Power Electronics*, vol. 12, no. 12, pp. 3295-3305, 16 10 2019.

[32] K. Nishida, T. Ahmed and M. Nakaoka, "Cost-Effective Deadbeat Current Control for Wind-Energy Inverter Application With LCL Filter," in *IEEE Transactions on Industry Applications*, vol. 50, no. 2, pp. 1185-1197, March-April 2014.

[33] R. N. Beres, X. Wang, F. Blaabjerg, M. Liserre and C. L. Bak, "Optimal Design of High-Order Passive-Damped Filters for Grid-Connected Applications," in *IEEE Transactions on Power Electronics*, vol. 31, no. 3, pp. 2083-2098, March 2016.

[34] H. Temiz, E. Demirok, O. Keysan, A. Türkay and B. Çetinkaya, "Performance comparison of passive series R and shunt R-C damped LCL filter for grid-connected inverters," in *The Journal of Engineering*, vol. 2019, no. 18, pp. 4698-4702, 7 2019.

[35] W. Wu, Y. He, T. Tang and F. Blaabjerg, "A New Design Method for the Passive Damped LCL and LLCL Filter-Based Single-Phase Grid-Tied Inverter," in *IEEE Transactions on Industrial Electronics*, vol. 60, no. 10, pp. 4339-4350, Oct. 2013.

[36] A. K. Balasubramanian and V. John, "Analysis and design of split-capacitor resistiveinductive passive damping for LCL filters in grid-connected inverters," in *IET Power Electronics*, vol. 6, no. 9, pp. 1822-1832, November 2013.

[37] W. Wu, Y. Liu, Y. He, H. S. Chung, M. Liserre and F. Blaabjerg, "Damping Methods for Resonances Caused by LCL-Filter-Based Current-Controlled Grid-Tied Power Inverters: An Overview," in *IEEE Transactions on Industrial Electronics*, vol. 64, no. 9, pp. 7402-7413, Sept. 2017.

[38] H. Ahn, C. Oh, W. Sung, J. Ahn and B. Lee, "Analysis and design of LCL filter with passive damping circuits for three-phase grid-connected inverters," *2015 9th International Conference on Power Electronics and ECCE Asia (ICPE-ECCE*

Asia), Seoul, 2015, pp. 652-658.

[39] J. Dannehl, M. Liserre and F. W. Fuchs, "Filter-Based Active Damping of Voltage Source Converters With LCL Filter," in *IEEE Transactions on Industrial Electronics*, vol. 58, no. 8, pp. 3623-3633, Aug. 2011.

[40] Won-Yong Sung, Hyo Min Ahn, Jung-Hoon Ahn, Chang-Yeol Oh and Byoung Kuk Lee, "Sensorless active damping method of LCL-filter in grid-connected parallel inverters for battery energy storage systems," *2017 IEEE 3rd International Future Energy Electronics Conference and ECCE Asia (IFEEC 2017 - ECCE Asia)*, Kaohsiung, 2017, pp. 1425-1429.

[41] W. Yao, Y. Yang, X. Zhang, F. Blaabjerg and P. C. Loh, "Design and Analysis of Robust Active Damping for LCL Filters Using Digital Notch Filters," in *IEEE Transactions on Power Electronics*, vol. 32, no. 3, pp. 2360-2375, March 2017.

[42] X. Zhou et al., "Robust Grid-Current-Feedback Resonance Suppression Method for LCL-Type Grid-Connected Inverter Connected to Weak Grid," in *IEEE Journal of Emerging and Selected Topics in Power Electronics*, vol. 6, no. 4, pp. 2126-2137, Dec. 2018.

[43] X. Wang, C. Bao, X. Ruan, W. Li and D. Pan, "Design Considerations of Digitally Controlled LCL-Filtered Inverter With Capacitor- Current-Feedback Active Damping," in *IEEE Journal of Emerging and Selected Topics in Power Electronics*, vol. 2, no. 4, pp. 972-984, Dec. 2014.

[44] M. T. Faiz et al., "Capacitor Voltage Damping Based on Parallel Feedforward Compensation Method for LCL-Filter Grid-Connected Inverter," in *IEEE Transactions on Industry Applications*, vol. 56, no. 1, pp. 837-849, Jan.-Feb. 2020.

[45] S. G. Parker, B. P. McGrath and D. G. Holmes, "Regions of Active Damping Control for LCL Filters," in *IEEE Transactions on Industry Applications*, vol. 50, no. 1, pp. 424-432, Jan.-Feb. 2014.

[46] M. Su et al., "Single-Sensor Control of LCL-Filtered Grid-Connected Inverters," in *IEEE Access*, vol. 7, pp. 38481-38494, 2019.

[47] S. Mariethoz and M. Morari, "Explicit Model-Predictive Control of a PWM Inverter With an LCL Filter," in *IEEE Transactions on Industrial Electronics*, vol. 56, no. 2, pp. 389-399, Feb. 2009.

[48] X. Hao, X. Yang, T. Liu, L. Huang and W. Chen, "A Sliding-Mode Controller

With Multiresonant Sliding Surface for Single-Phase Grid-Connected VSI With an LCL Filter," in *IEEE Transactions on Power Electronics*, vol. 28, no. 5, pp. 2259-2268, May 2013.

[49] M. T. Bina and A. K. S. Bhat, "Averaging Technique for the Modeling of STATCOM and Active Filters," in *IEEE Transactions on Power Electronics*, vol. 23, no. 2, pp. 723-734, March 2008.

[50] Zhaoan Wang, Qun Wang, Weizheng Yao and Jinjun Liu, "A series active power filter adopting hybrid control approach," in *IEEE Transactions on Power Electronics*, vol. 16, no. 3, pp. 301-310, May 2001.

[51] E. R. Ribeiro and I. Barbi, "Harmonic Voltage Reduction Using a Series Active Filter Under Different Load Conditions," in *IEEE Transactions on Power Electronics*, vol. 21, no. 5, pp. 1394-1402, Sept. 2006.

[52] J. Barros and E. Perez, "An adaptive method for determining the reference compensating current in single-phase shunt active power filters," *in IEEE Transactions on Power Delivery*, vol. 18, no. 4, pp. 1578-1580, Oct. 2003.

[53] M. Cirrincione, M. Pucci, G. Vitale and A. Miraoui, "Current Harmonic Compensation by a Single-Phase Shunt Active Power Filter Controlled by Adaptive Neural Filtering," in *IEEE Transactions on Industrial Electronics*, vol. 56, no. 8, pp. 3128-3143, Aug. 2009.

[54] Z. Shuai, A. Luo, W. Zhu, R. Fan and K. Zhou, "Study on a Novel Hybrid Active Power Filter Applied to a High-Voltage Grid," in *IEEE Transactions on Power Delivery*, vol. 24, no. 4, pp. 2344-2352, Oct. 2009.

[55] A. M. Al-Zamil and D. A. Torrey, "A passive series, active shunt filter for high power applications," in *IEEE Transactions on Power Electronics*, vol. 16, no. 1, pp. 101-109, Jan. 2001.

[56] L. Wang, C. Lam and M. Wong, "Hybrid Structure of Static Var Compensator and Hybrid Active Power Filter (SVC//HAPF) for Medium-Voltage Heavy Loads Compensation," in *IEEE Transactions on Industrial Electronics*, vol. 65, no. 6, pp. 4432-4442, June 2018.

[57] L. Wang, C. Lam and M. Wong, "Unbalanced Control Strategy for A Thyristor-Controlled LC-Coupling Hybrid Active Power Filter in Three-Phase Three-Wire Systems," in *IEEE Transactions on Power Electronics*, vol. 32, no. 2, pp. 1056-1069, Feb. 2017.

[58] B. Cao, L. Chang and R. Shao, "Predictive Current Controller for Single-Phase Grid-Connected VSIs With Compensation for Time-Delay Effect and System Uncertainty," in *IEEE Journal of Emerging and Selected Topics in Power Electronics*, vol. 6, no. 4, pp. 1761-1768, Dec. 2018.

[59] Heng Deng, R. Oruganti and D. Srinivasan, "PWM methods to handle time delay in digital control of a UPS inverter," in *IEEE Power Electronics Letters*, vol. 3, no. 1, pp. 1-6, March 2005.

[60] Y. Guan, Y. Wang, Y. Xie, Y. Liang, A. Lin and X. Wang, "The Dual-Current Control Strategy of Grid-Connected Inverter With LCL Filter," in *IEEE Transactions on Power Electronics*, vol. 34, no. 6, pp. 5940-5952, June 2019.(weak grid)

[61] S. N. Vukosavić and L. S. Perić, "Modified digital current controller with reduced impact of transport delays," in *IET Electric Power Applications*, vol. 10, no. 6, pp. 517-525, 7 2016.

[62] J. Wang, J. D. Yan, L. Jiang and J. Zou, "Delay-Dependent Stability of Single-Loop Controlled Grid-Connected Inverters with LCL Filters," in *IEEE Transactions on Power Electronics*, vol. 31, no. 1, pp. 743-757, Jan. 2016.

[63] J. Yin, S. Duan and B. Liu, "Stability Analysis of Grid-Connected Inverter With LCL Filter Adopting a Digital Single-Loop Controller With Inherent Damping Characteristic," in *IEEE Transactions on Industrial Informatics*, vol. 9, no. 2, pp. 1104-1112, May 2013.

[64] D. Pan, X. Ruan and X. Wang, "Direct Realization of Digital Differentiators in Discrete Domain for Active Damping of LCL -Type Grid-Connected Inverter," in *IEEE Transactions on Power Electronics*, vol. 33, no. 10, pp. 8461-8473, Oct. 2018.

[65] X. Chen, Y. Zhang, S. Wang, J. Chen and C. Gong, "Impedance-Phased Dynamic Control Method for Grid-Connected Inverters in a Weak Grid," in *IEEE Transactions on Power Electronics*, vol. 32, no. 1, pp. 274-283, Jan. 2017.

[66] Y. He, H. S. Chung, C. Lai, X. Zhang and W. Wu, "Active Cancelation of Equivalent Grid Impedance for Improving Stability and Injected Power Quality of Grid-Connected Inverter Under Variable Grid Condition," in *IEEE Transactions on Power Electronics*, vol. 33, no. 11, pp. 9387-9398, Nov. 2018.

[67] J. Fang, X. Li, X. Yang and Y. Tang, "An Integrated Trap-LCL Filter With

Reduced Current Harmonics for Grid-Connected Converters Under Weak Grid Conditions," in *IEEE Transactions on Power Electronics*, vol. 32, no. 11, pp. 8446-8457, Nov. 2017.

[68] H. Azani, A. Massoud, L. Benbrahim, B. W. Williams and D. Holiday, "An LCL filter-based grid-interfaced three-phase voltage source inverter: Performance evaluation and stability anaylsis," *7th IET International Conference on Power Electronics, Machines and Drives (PEMD 2014)*, Manchester, 2014, pp. 1-6.

[69] S. Silwal, S. Taghizadeh, M. Karimi-Ghartemani, M. J. Hossain and M. Davari, "An Enhanced Control System for Single-Phase Inverters Interfaced With Weak and Distorted Grids," in *IEEE Transactions on Power Electronics*, vol. 34, no. 12, pp. 12538-12551, Dec. 2019.

[70] K. Nishida, M. Rukonuzzaman and M. Nakaoka, "Digital control three-phase shunt active power filter with a new harmonic-current-extraction process," in *IEE Proceedings - Generation, Transmission and Distribution*, vol. 152, no. 4, pp. 529-538, 8 July 2005.

[71] W. U. K. Tareen and S. Mekhielf, "Three-Phase Transformerless Shunt Active Power Filter With Reduced Switch Count for Harmonic Compensation in Grid-Connected Applications," in *IEEE Transactions on Power Electronics*, vol. 33, no. 6, pp. 4868-4881, June 2018.

[72] S. Bosch, J. Staiger and H. Steinhart, "Predictive Current Control for an Active Power Filter With LCL-Filter," in *IEEE Transactions on Industrial Electronics*, vol. 65, no. 6, pp. 4943-4952, June 2018.

[73] X. Zhang, J. He, CHUNG and S. Henry, "Generic Stability Impedance Criterion for the Parallel Inverters System," *2018 IEEE 4th Southern Power Electronics Conference (SPEC)*, Singapore, Singapore, 2018, pp. 1-4.

[74] Y. Chen, J. M. Guerrero, Z. Shuai, Z. Chen, L. Zhou and A. Luo, "Fast Reactive Power Sharing, Circulating Current and Resonance Suppression for Parallel Inverters Using Resistive-Capacitive Output Impedance," in *IEEE Transactions on Power Electronics*, vol. 31, no. 8, pp. 5524-5537, Aug.

[75] Q. Zhong and Y. Zeng, "Universal Droop Control of Inverters With Different Types of Output Impedance," in *IEEE Access*, vol. 4, pp. 702-712, 2016.

[76] Y. Qi and Y. Tang, "Enhancing the Harmonic Current Sharing Performance of Low-Switching-Frequency Inverters Though Dynamic Impedance

Reshaping," *2018 IEEE Energy Conversion Congress and Exposition (ECCE)*, Portland, OR, 2018, pp. 3150-3155.

[77] T. Wu, C. Kuo, K. Sun and H. Hsieh, "Combined Unipolar and Bipolar PWM for Current Distortion Improvement During Power Compensation," in *IEEE Transactions on Power Electronics*, vol. 29, no. 4, pp. 1702-1709, April 2014.